VU VRIJE UNIVERSITEIT AMSTERDAM

VU Research Portal

Provenance and sedimentology of Red Clay and loess in northern China

Shang, Y.

2018

document version
Publisher's PDF, also known as Version of record

Link to publication in VU Research Portal

citation for published version (APA)
Shang, Y. (2018). *Provenance and sedimentology of Red Clay and loess in northern China*. [PhD-Thesis - Research and graduation internal, Vrije Universiteit Amsterdam].

General rights
Copyright and moral rights for the publications made accessible in the public portal are retained by the authors and/or other copyright owners and it is a condition of accessing publications that users recognise and abide by the legal requirements associated with these rights.

- Users may download and print one copy of any publication from the public portal for the purpose of private study or research.
- You may not further distribute the material or use it for any profit-making activity or commercial gain
- You may freely distribute the URL identifying the publication in the public portal ?

Take down policy
If you believe that this document breaches copyright please contact us providing details, and we will remove access to the work immediately and investigate your claim.

E-mail address:
vuresearchportal.ub@vu.nl

Download date: 04. May. 2023

VRIJE UNIVERSITEIT

PROVENANCE AND SEDIMENTOLOGY OF RED CLAY AND LOESS IN NORTHERN CHINA

ACADEMISCH PROEFSCHRIFT

ter verkrijging van de graad Doctor aan
de Vrije Universiteit Amsterdam,
op gezag van de rector magnificus
prof.dr. V. Subramaniam,
in het openbaar te verdedigen
ten overstaan van de promotiecommissie
van de Faculteit der Bètawetenschappen
op dinsdag 6 februari 2018 om 13.45 uur
in de aula van de universiteit,
De Boelelaan 1105

door

Yuan Shang

geboren te Tianshui, China

promotoren: prof.dr. R.T. van Balen

copromotoren: dr. M.A. Prins
dr. C.J. Beets
dr. A.P. Kaakinen

Reading committee:

prof.dr. J.R. Wijbrans
prof.dr. H.Y. Lu
prof.dr. H. Renssen
dr. T. Stevens
dr. J-B. Stuut

This dissertation is the result of a double doctorate program carried out at:

Vrije Universiteit Amsterdam
Faculty of Science
Department of Earth Sciences
Amsterdam, the Netherlands
&
University of Helsinki
Faculty of Science
Department of Geosciences and Geography
Helsinki, Finland

© Yuan Shang, 2018

Cover design and Layout: Yuan Shang
Cover photo: Anu Kaakinen
Printed by: Ipskamp Printing
ISBN: 978-94-028-0913-8

Contents

Acknowledgements

This work started four years ago as a double doctorate program, carried out at the University of Helsinki in Finland and Vrije Universiteit Amsterdam, in the Netherlands. Accomplishing of this thesis in the two beautiful countries is a very unique and memorable experience for me. A great many people have offered their expertise and knowledge, support and inspiration over the course of this journey. Here, I would like to take this opportunity to express my sincere gratitude to them:

First and foremost, I am deeply indebted to my supervisor Dr. Anu Kaakinen. My PhD study would have never begun without Anu's kindly reply to my email in the spring of 2013. She introduced me to the world of research and provided me with the opportunity to work in a wonderful international project. It would be impossible to finish this PhD thesis without her constant support and contribution. I greatly appreciate the enormous time and patience she spent on mentoring me. She has always been positive and had faith in my work which significantly improved my confidence in doing research and motivated me to continue.

I was fortunate to work with other two brilliant supervisors Dr. Maarten A. Prins and Dr. Christiaan J. Beets in the Netherlands. I highly appreciate them for sharing their expertise, wisdom and time over the years. Their contribution and support during all the stages of this work has been of invaluable help. Many ideas were born during the inspiring discussions with them. I have been constantly impressed by their broad knowledge in the field and new perspectives in the research topic. Maarten and Kay, thanks for hosting me in VU and introducing me the colleagues there. Those "sightseeing tours" we had together in the Netherlands were really fun and a nice memory for me.

I am grateful to my VU promoter Prof. Ronald van Balen who was extremely helpful especially during the final stages of this work. Many thanks are owed to Prof. Mikael Fortelius in the University of Helsinki for his support and encouragement over the course of this project.

I wish to thank all the co-authors for collaboration, for helping with fieldwork, laboratory analyses and their contribution at various stages of the manuscripts. My special thanks are directed to Dr. Hui Tang, Dr. Bin Wang and Dr. Tobias Fusswinkel for fruitful discussions and sharing their scientific expertise and skills.

I would like to thank the members of the dissertation reading committee: Prof. H.Y. Lu, Prof. H. Renssen, Dr. T. Stevens, Dr. J-B. Stuut and Prof. J.R. Wijbrans for assessing the quality of this thesis and providing helpful comments.

I acknowledge the GeoDoc programme of the University of Helsinki for the financial support of several international conferences and other research visits abroad. I received the thesis completion grant from the University of Helsinki that enabled me to finalise this thesis.

I had great time in working at the Geological Survey of Finland (GTK) in Espoo where I produced the extensive zircon U-Pb age dataset for my thesis. I want to thank the people there for their support and assistance. Especially, Dr. Yann Lahaye, Dr. Hugh O 'Brien and Dr. Marja Lehtonen are highly appreciated for the time spending on my project and detailed guidance for the using of ICP-MS and SEM imaging and related data reduction.

I am much obliged to the colleagues and personnel in the Department of Geosciences and Geography, University of Helsinki who have made my work and life much easier and with a lot of fun. I send my gratitude to Prof. Tapani Rämö for his helpful suggestions in improving my first manuscript and for his interest of my project. I am grateful to Dr. Seija Kultti and Dr. Mia Kotilainen for their valuable advices and support related to my PhD study. I thank all the officemates (present and past) in C118: Outi Hyttinen, Leena Sukselainen, Paula Salminen, Bin Wang, and Joonas Wasiljeff for sharing the office and many joyful scientific and non-scientific conversations. I send my gratitude to Heikki Seppä, Juha Karhu, Tino Johansson, Helena Korkka, Aku Heinonen, Indrė Žliobaitė, Tuija Vaahtojärvi, Pasi Heikkilä, Mikko Haaramo, Hanna Reijola and Juhani Virkanen for various support and help. I would like to thank Marttiina Rantala, Mimmi Oksman, Ferhat Kaya, Yurui Zhang, Henrik Kalliomäki, Stefan Andersson, Radoslaw Michallik, Janina Rannikko, Liisa Ilvonen, Aleksis Karme, Normunds Stivrins, Peter Howett, Minja Seitsamo-Ryynänen and others for their friendship and vital peer support.

Benefited from this joint PhD project, I visited the Department of Earth Sciences, Vrije Universiteit Amsterdam quite often. I met many friendly and helpful people there and I wish to send my gratitude to them. In particular, I want to thank Roel van Elsas, chef of the mineral separation laboratory, for vital technical support and guidance. Roel is just capable of solving everything in the lab! Roel, thanks for taking me to the hospital when I accidently burned my arm. I want to thank Martine Hagen and Tineke Vogel-Eissens for assistance in grain size analysis and zircon separation. Tineke, it was a great experience to cycle with you in the beautiful countryside of Holland! My thanks also goes to Dr. Daniel Rits for helping me with many practical issues in VU.

Besides all my colleagues, I wish to thank my friends. My special thanks go to my badminton friends that have played the game with me weekly in Kumpula Unisport. I give my sincere gratitude to my Chinese friends both in Helsinki and Amsterdam. Thanks for sharing the delicious food, accompanying in holidays and events. All the activities we had together have enriched my life and enabled me to get rid of loneliness when studying abroad. In particular, I would like to thank Zhang Jun, Yu Liang, Li Huan, Sun Xilin and Peng Fei for friendship and sharing their lives with me in Amsterdam.

Last but not the least, I send my deepest gratitude to my family for their endless love and unconditional trust. I dedicate this thesis to them.

Summary

Red Clay and overlying loess-palaeosol sequences are typical for the area in Northern China that is known as the Chinese Loess Plateau (CLP). These primarily aeolian sediments provide one of the best terrestrial archives of Neogene-Quaternary climate change, and their formation has been linked to the uplift of the Tibetan Plateau, the progressive aridification of East Asia and the onset of and changes in the East Asian monsoon. In the present study, the sediment provenance was reconstructed using a combination of analytical techniques that allowed better understanding of the (long-term) shifts in sediment delivery in response to changes in the climate and tectonic evolution.

Zircon U–Pb age spectral and backtrace trajectory modelling of three well known Red Clay sequences distributed across the CLP revealed the spatiotemporal variations in the provenance of late Miocene-Pliocene Red Clay. The results indicated that the Red Clay in the southern and western CLP was mainly derived from the Northern Tibetan Plateau (NTP) and the Taklimakan Desert. In contrast Red Clay in the northeastern CLP displays a zircon U-Pb age signature of the broad area of the Central Asian Orogenic Belt. In addition, the north-eastern Red Clay shows increased contributions from the west around 3.6 Ma, possibly suggesting an intensified westerly wind strength and/or aridity of the NTP and Taklimakan Desert arising from the uplift of the NTP and Tianshan Mountains in the Pliocene. This could also be caused by the onset of enhanced Yellow River drainage in response to the increased NTP denudation since 3.6 Ma.

To further investigate the role of the Yellow River in supplying dust to the Quaternary loess deposits, the sedimentology and source signal of the unique loess-palaeosol sequence of the Mangshan Loess Plateau (MLP) along the lower reach of the Yellow River was investigated by end-member modelling of the loess grain-size records and single-grain zircon U-Pb dating. The results suggest that the Yellow River floodplain north of the MLP has served as a major dust source at least since 900 ka. The sudden change in sedimentology (accumulation rate, grain-size distribution) of the Mangshan sequence above palaeosol unit S2 may have been initiated by a combination of tectonic movements in the Weihe Basin and in the Yellow River floodplain north of the MLP around 240 ka. Subsequent rapid fluvial incision in the northern part of the Weihe Basin resulted in increased sediment flux being transported to the lower reach of the Yellow River. Tectonic movements in the floodplain north of the MLP would have caused a southward migration of the Yellow River course, explaining the formation of an impressive scarp and the more proximal location of the sediment source.

In addition to provenance analysis, grain size and shape characteristics obtained by dynamic image analysis (DIA) were used to fingerprint the transport processes of silt particles in a series of Quaternary loess-palaeosol sequences. The results revealed a decrease in the aspect ratio of the particles as a function of increasing grain size, thus indicating that systematic shape sorting occurred during the aeolian transport of the silt particles. A similar particle-shape sorting trend has also been found in a series of Red Clay

sequences, confirming that the Red Clay deposits are predominantly of aeolian origin. This study indicates that DIA of grain size and shape characteristics can be an additional powerful tool for fingerprinting trends in grain size and shape sorting, determining the dominant mode of transport, and reconstructing the transportation pathways of silt-sized aeolian sediments.

The final part of this thesis comprised a pilot study on the use of the trace-element composition of quartz as a provenance tool to constrain the source area of the late Neogene and Quaternary dust deposits in Northern China. It revealed that quartz in the Mangshan loess deposits is largely derived from the Qaidam Basin of the NTP. The likely dust contribution from the Taklimakan Desert to the Red Clay deposits in Baode is also reflected in the trace element content of quartz. These results are comparable with the source signal obtained from the zircon U-Pb age spectra, suggesting that the trace element composition of quartz could be applied as an alternative tool to other single-grain provenance analytical approaches to track the dust source and dust pathways of the aeolian sediments.

Samenvatting

Rode klei en overliggende löss sequenties zijn kenmerkend voor het gebied in Noord-China dat bekend staat als het Chinese Löss Plateau (CLP). Deze voornamelijk eolische sedimenten met de daarin gevormde (fossiele) bodems leveren een van de beste terrestrische archieven van de Neogene en Kwartaire klimaatveranderingen. De vorming is gekoppeld aan de opheffing van het Tibetaanse plateau, de geleidelijke opdroging van Oost-Azië en het begin van, en de veranderingen in de Oost-Aziatische moesson. In deze voorliggende studie wordt de herkomst van dit sediment gereconstrueerd met behulp van een combinatie van analytische technieken die het mogelijk maakt om de (lange termijn) verschuivingen in sedimentaanvoer en afzetting beter te begrijpen als reactie op veranderingen in het klimaat en de tektonische evolutie van het gebied.

Het modelleren van zirkoon U-Pb ouderdom spectra en afgeleide transportbanen van drie bekende Rode Klei-sequenties verdeeld over het CLP onthullen de spatio-temporele variaties in de herkomst van deze laat Miocene-Pliocene afzettingen. Ze geven aan dat de Rode Klei in het zuidelijke en westelijke CLP voornamelijk afkomstig is van het noordelijke Tibetaanse plateau (NTP) en de Taklimakan-woestijn. Rode Klei in het noordoosten van het CLP vertoont daarentegen een zirkoon U-Pb daterings-signatuur van het brede gebied van de Centraal-Aziatische orogene gordel. Daarnaast vertoont de noordoostelijke Rode Klei afgezet rond 3,6 miljoen jaar geleden een verhoogde bijdrage vanuit het westen, hetgeen mogelijk duidt op een geïntensiveerde westelijke windsterkte en/of droogte van het NTP en de Taklimakan-woestijn als gevolg van de opheffing van het NTP- en de Tianshan-bergen in het Plioceen. Dit kan ook worden veroorzaakt door het begin van een toegenomen Gele Rivier-afvoer als reactie op de toegenomen NTP-denudatie sinds 3.6 miljoen jaar geleden.

Om de rol van de Gele Rivier bij het leveren van stof aan de Kwartaire löss-afzettingen verder te onderzoeken, is de sedimentologie en het bronsignaal van de unieke löss-fossiele bodem sequentie van het Mangshan Löss Plateau (MLP) langs het lagere bereik van de Gele Rivier, bestudeerd met de eindlid modellering van de löss korrelgrootte gegevens en zirkoon-U-Pb-dateringen. De resultaten suggereren dat de riviervlakte van de Gele Rivier ten noorden van het MLP ten minste sinds 900 ka als belangrijkste stofbron heeft gediend. De plotselinge verandering in sedimentologie (accumulatiesnelheid toename, korrelgrootteverdeling vergroving) van de Mangshan-sequentie boven de fossiele S2 bodem kan het gevolg zijn van een combinatie van tektonische bewegingen in het Weihe-bekken en in de stroomvlakte van de Gele Rivier ten noorden van de MLP rond 240 ka. Daaropvolgende snelle rivier insnijding in het noordelijke deel van het Weihe-bekken resulteerde in een verhoogde sedimentstroom die naar het lagere bereik van de Gele Rivier werd getransporteerd. Tektonische bewegingen in de riviervlakte ten noorden van het MLP zouden een zuidwaartse migratie van de Gele Rivier hebben veroorzaakt, wat de vorming van een indrukwekkende steilwand en de meer proximale locatie van de sedimentbron verklaart.

Naast de herkomstanalyse worden korrelgrootte- en vormkarakteristieken, verkregen door dynamische beeldanalyse (DIA), gebruikt om de transportprocessen van de silt deeltjes in een reeks Kwartaire löss-fossiele bodem sequenties te duiden. De resultaten onthullen dat de aspect-ratio van de deeltjes afneemt met toenemende korrelgrootte, hetgeen dus aangeeft dat er een systematische vormsortering plaatsvond tijdens het eolische transport van de deeltjes. Een vergelijkbare sorteringstrend is ook gevonden in een reeks Rode Klei-opeenvolgingen, wat bevestigt dat deze afzettingen overwegend van een eolische oorsprong zijn. Deze studie geeft aan dat DIA van korrelgrootte- en vormkarakteristieken een krachtig hulpmiddel kan zijn voor het vaststellen van korrelgrootte- en vormsorteringstrends, het bepalen van de dominante transportmodus en het reconstrueren van de transportroutes van siltige eolische sedimenten.

Het laatste deel van dit proefschrift is een eerste studie naar het gebruik van de sporenelementen-samenstelling van kwarts als herkomst hulpmiddel om het brongebied van de laat Neogene en Kwartaire stofafzettingen in Noord-China vast te stellen. Het laat zien dat kwarts in de Mangshan lössafzettingen grotendeels afkomstig zijn uit het Qaidam-bekken van het NTP. De waarschijnlijke stofbijdrage van de Taklimakan-woestijn aan de Rode Klei-afzettingen in Baode wordt ook weerspiegeld in het gehalte aan sporenelementen van kwarts. Deze resultaten zijn vergelijkbaar met het bronsignaal verkregen uit de zirkoon U-Pb-daterings-spectra, wat suggereert dat de samenstelling van sporenelementen van kwarts zou kunnen worden toegepast als een alternatief hulpmiddel om de bron en transportpaden van de eolische afzettingen te bepalen.

Chinese Summary

摘 要

中国北方分布着世界上最厚，最为连续的风尘沉积-黄土和红粘土序列。这些沉积物蕴含着丰富的古环境变化信息。对于这些风尘物的物源变化研究不仅在于揭示它们的产生和搬运机制，更有助于我们理解晚新生代以来亚洲内陆风尘源区的干旱化过程以及大气环流格局的变迁。本论文通过分析中国黄土高原的黄土和红粘土剖面的沉积特征，综合使用传统和新型的沉积学和物源示踪方法来重建晚新近纪以来黄土高原风尘沉积物物源的时空变化及其传输路径，并探讨它们对于气候变化和构造演化的响应。

论文首先对黄土高原三个典型的晚中新世–上新世红粘土剖面（保德、蓝田以及董湾）进行物源的时空变化分析。本研究使用碎屑锆石的U-Pb年龄来约束沉积物的物源变化以及利用粒度端元模型（End member modelling）来分析红粘土的不同动力组分及其运移过程并结合回溯轨迹模型（backtrace trajectory modelling）来重建晚中新世的风尘传输路径。结果表明：青藏高原东北部（包括祁连山和柴达木盆地）的风化物是黄土高原西部（董湾）和南部（蓝田）风成红粘土的主要物源。此外塔克拉玛干沙漠的风尘输送也可能对董湾和蓝田红粘土中的细颗粒组分有所贡献。相反，黄土高原东北部的保德红粘土（保德组和静乐组），其风尘来源除了有来自青藏高原东北部的物质外，中亚造山带的风化物也是其组成成分。与黄土物源的研究对比发现，红粘土在物源上的空间异质性与第四纪黄土是一致的。我们还发现自3.6 Ma以来，静乐组红粘土中关于其西部物源区（青藏高原东北部和塔克拉玛干沙漠）的锆石年龄信号增加，表明更多物质从西部干旱区输送而来。这可能与上新世以来青藏高原以及天山的隆起所造成的西部干旱化加剧以及近地面的西风加强有关。此外，3.6 Ma 以来由于青藏高原的快速隆起，导致黄河从青藏高原向其冲积平原的物质输送增加，也可能是引起西部物源增加的原因。

为了进一步研究黄河对于中国北方第四纪风尘沉积的物质输送，我们选取了位于黄河下游的邙山塬的黄土–古土壤序列，对其沉积特征（粒度和沉积速率）和物源变化进行分析。邙山黄土剖面在古土壤层S2之上呈现出粗颗粒组分和沉积速率明显增加的趋势。以单颗粒锆石U-Pb年龄为依据的物源信号显示邙山黄土从黄土层L9沉积开始，其物源无明显变化；邙山黄土塬北部的黄河河漫滩是自黄土层L9沉积开始邙山风尘沉积物最主要的物源区。这暗示着黄河至少在L9沉积时已经贯穿三门峡，即黄河中游和下游贯通的时间应早于900 ka。邙山黄土–古土壤序列在古土壤层S2之上出现的剧烈的沉积特征的变化可能是由于渭河盆地在240 ka 发生的构造运动引起盆地北部河流下切，侵蚀加剧，造成更多的物质被输送到黄河下游所致。此外这一时期的构造运动可能导致黄河河道向南迁移，使黄河河漫滩更接近邙山塬，从而形成一个更近的物源区也是邙山S2以上粗颗粒组分增加的原因。

论文第四章使用动态图像分析方法（dynamic image analysis，DIA ）对黄土高原

黄土和红粘土沉积物的粒度和粒型进行分析并通过观察风尘沉积物中粉砂粒级的粒度–粒型的分布特征来研究其传输路径及运移过程。本研究发现黄土中粉砂粒级的颗粒物的长宽比随粒度的增加而减小，表明颗粒在风力运输过程中存在系统的形状分选。红粘土的粒度–粒型分布也呈现相同趋势，这意味着红粘土与黄土一样，均为风尘沉积物，其颗粒物的运移和黄土遵循同样的规律。

论文的最后一部分为使用碎屑石英中微量元素的含量来约束中国北方晚新近纪和第四纪风尘沉积物物源的初步研究。结果显示邙山黄土中石英颗粒的微量元素含量与青藏高原北部和柴达木盆地的碎屑物中的类似。此外，塔克拉玛干沙漠对保德红粘土的风尘贡献也反映在石英的微量元素含量上。这些结果与碎屑锆石U-Pb年龄所指征的物源信号具有可比性。本研究表明单颗粒石英中的微量元素含量可以作为风尘沉积物源区示踪的潜在研究方法。

Chapter 1

Introduction

1.1. Background

Airborne mineral dust generated from arid and semi-arid regions, once uplifted into the atmosphere, plays a significant role in the Earth system (Knippertz and Stuut, 2014). It interacts with climate by affecting the radiative budget, modifying atmospheric chemistry and contributing micronutrients to both terrestrial and marine ecosystems (Swap et al., 1992; Dentener et al., 1996; Balkanski et al., 2007; Schroedter-Homscheidt et al., 2013). In addition to the climate influence, dust and dust storms could also have severe environmental consequences along the transport pathways, such as affecting local air quality and impacting on human health by causing respiratory diseases and infections (Prospero et al., 2008). Dust records of the past, on the other hand, provide us with vital information on dust-related aspects of the Earth system over time, such as wind strength, atmospheric circulation patterns and variations in the vegetation cover. The Asian dry interior is regarded as one of the most important dust sources. Aeolian dust emitted from the Asian interior can be transported to proximal downwind regions such as the Chinese Loess Plateau (CLP) in northern China and further eastwards over the Pacific Ocean and onwards onto the Greenland ice cap (Sun et al., 2001; Sugimoto et al., 2002). Notably thick and continuous dust deposits have accumulated in the CLP at least since the late Oligocene (Heller and Liu, 1982; Guo et al., 2002; Qiang et al., 2011). It has been suggested that the onset and formation of the aeolian deposits in the CLP have been affected by two remarkable processes during the Cenozoic: phased uplift of the Tibetan Plateau and Northern Hemisphere glaciation. In addition, both of these could have shaped the winds that transport the aeolian dust to the CLP (An et al., 2001). Deciphering such long terrestrial dust records would aid us in understanding the coupled effect of tectonic activity and regional climate on the changes in Earth surface processes during the Cenozoic. Knowledge of the dust provenance is the essential first step in exploring the whole dust pathway from source to sink. While contemporary dust sources can be recognised by means of Earth-orbiting satellites (Crusius et al., 2011; Prospero et al., 2012; Muhs et al., 2014), detecting the source areas of the palaeo-dust is not so straightforward.

Typically, dust records of the CLP are divided into three sequences: 1) Miocene loess (in the west of the Liupan Mountains; Fig.1.1), 2) Late Miocene-Pliocene Red Clay and 3) Quaternary loess-palaeosol (Liu, 1985; Guo et al., 2002; An et al., 2014). Loess is typically composed of silt-sized sediment particles and accumulated during glacial intervals when the Asian interior was colder and drier, while the palaeosols developed during interglacial periods when climate conditions were warmer and more humid. Red

Clay is commonly regarded as a thick, fossiliferous, reddish soil complex primarily composed of clay and fine silt particles (Ding et al., 1998). While loess is considered to be of exclusively windblown origin, the bottom part of Red Clay deposits in some sites has been argued to be of fluvial origin or reworked by fluvial process (Guo et al., 2001; Alonso-Zarza et al., 2009; Zhang et al., 2013b; Nie et al., 2014). Nevertheless, the main body of the Red Clay sequences has been well acknowledged as being of aeolian origin, based on field observations and grain-size, geochemical and magnetic property analysis (Sun et al., 1997; Ding et al., 1998; An et al., 2001; Ding et al., 2001a; Guo et al., 2001; Lu et al., 2001; An et al., 2014). Inferred from the modern dust observations, dust on the CLP has been suggested to be generated from the arid Asia interior through transportation by near-surface winds of the winter monsoon resulting from the Siberian–Mongolian high-pressure system and/or westerly jet (Ding, 2005; Roe, 2009). Following this regime, a large number of arid regions located west and north of the CLP that are capable of producing silts could be potential source areas for the CLP dust (Fig.1.1). These arid regions are characterised by a range of landscapes, such as high mountains, gobi (stony desert) and sandy lands, fluvial fans, yardangs, playas and piedmonts (Pye and Zhou, 1989; Pye, 1995; Sun et al., 2002; Smalley et al., 2009).

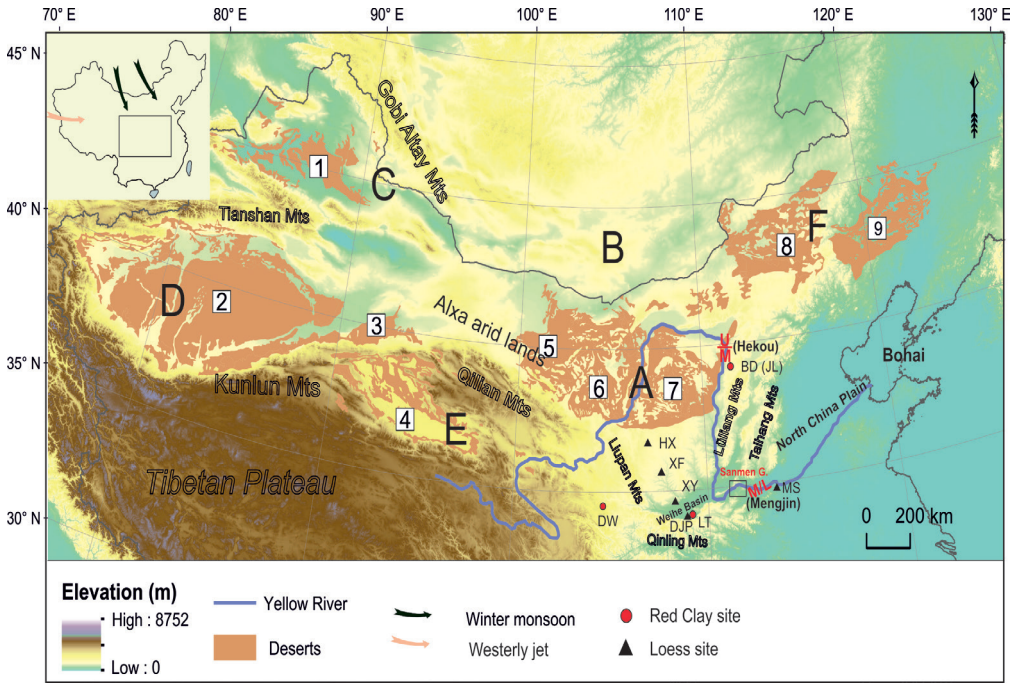

Figure 1.1. Map of northern China. Number 1-9 indicates the major deserts in western, northern and eastern parts of the CLP. 1 -Gurbantunggut (Jungger Basin), 2 - Taklimakan (Tarim Basin), 3 - Kumtag, 4 - Qaidam, 5 - Badain Jaran, 6 - Tengger, 7 - Mu Us, 8 -Otindag and 9 - Horqin. The black triangles mark the loess sections while the red dots indicate the Red Clay sites of this study. HX-Huanxian, XF- Xifeng, XY - Xunyi, DJP - Duanjiapo, MS - Mangshan, DW - Dongwan, LT - Lantian, BD - Baode and JL - Jingle. A–F indicate the grouped potential source areas for the CLP. A - adjacent deserts north and northwest of the CLP; B -southern Mongolia Desert; C - Jungger Basin and Gobi Altay Mountains; D - Taklimakan Desert; E - Northern Tibetan Plateau, including Qilian Mountains and Qaidam Basin; F - deserts northeast of the CLP. The red letters indicate the boundaries of the upper and middle reaches and the middle and lower reaches of the Yellow River.

The source, or sources, of the aeolian loess in the CLP have been disputed for decades. Previous studies based on grain-size records of the loess-palaeosol sequences have demonstrated that in the central CLP the loess grain size shows an approximately north–south decreasing trend, particularly during glacial intervals. Systematic decreases in the loess thickness have been observed along the same transect as a consequence of sediment load reduction in a downwind direction (Pye, 1995; Ding et al., 2002; Nugteren and Vandenberghe, 2004; Prins and Vriend, 2007). These observations suggest a dominant north–south dust transport pathway for loess deposits in the CLP and the presence of a proximal dust source or sources north and northwest of the CLP. Based on isotopic, geochemical and mineralogigal analyses, Sun (2002) proposed that the gobi in southern Mongolia and the adjacent gobi and sandy deserts of northern and northwest China (the Badain Jaran, Tengger, Ulan Buh, Hubq and Mu Us Deserts) are the main source areas for the CLP loess, rather than the three inland basins: the Tarim, Qaidam and Jungger Basins (Fig.1.1). However, Sun (2002) pointed out that those deserts actually acted as the source holding areas rather than the dust producers. According to Sun (2002), silts in the CLP dust records are ultimately produced from high mountain ranges ("High Asia") such as the Gobi Altay Mountains and Qilian Mountains during "mountain processes" (i.e. glacial grinding, tectonic processes, frost weathering, salt weathering and fluvial comminution). The provenance signal inferred from radiogenic isotope data ($^{87}Sr/^{86}Sr$ and $^{143}Nd/^{144}Nd$) suggests that the "western deserts", the deserts and arid lands located west of the CLP (Qaidam Basin, Badain Jaran Desert and Tengger Desert), rather than the "northern deserts" (Hobq desert and Mu Us Desert) were the main source regions for the CLP dust during glacial stages (Chen et al., 2007). A recent study based on the same methods also pointed out a constant dust supply to the CLP from the region between the Qilian Mountains and Gobi Altay Mountains, i.e., the Alxa arid lands, since the early Miocene (Chen and Li, 2013).

In recent years, the application of single-grain zircon U-Pb dating techniques has allowed the discrimination of multiple potential source areas for the CLP dust. The advantage of single-grain analysis in provenance studies over bulk analysis techniques is that it will not average out signatures from multiple source areas. Zircon U-Pb chronology has revealed a significant dust supply from the northern and north-eastern Tibetan Plateau and Qaidam Basin, mixed with additional contributions from the Gobi Altay Mountains and Northern China Craton to the CLP loess deposits (Pullen et al., 2011; Che and Li, 2013; Stevens et al., 2013; Bird et al., 2015; Licht et al., 2016b; Zhang et al., 2016). Moreover, the zircon U-Pb age spectra also indicate spatial variation in the dust source of the loess deposits across the CLP (Bird et al., 2015), although whether there are any temporal (e.g. glacial/interglacial) variations in the provenance of loess-palaeosol sequences remains uncertain and debated (Xiao et al., 2012; Che and Li, 2013; Bird et al., 2015; Licht et al., 2016b).

What is still ambiguous is how the sediments were transported from the source area(s) to the CLP. Some studies have advocated direct transport from the north and northwest by winds passing Mu Us Desert, Tengger Desert and Badain Jaran Desert during interglacial stages, and from the west through the Qaidam Basin and Qilian Mountains during glacial stages (Kapp et al., 2011; Pullen et al., 2011). However, inferred from the results of

mixing modelling on the loess grain-size dataset, Prins et al. (2007) and Prins and Vriend (2007) suggested the opposite pattern. Others have addressed the significant contribution of Yellow River sediments to the CLP dust based on the zircon age provenance data. They have interpreted that the sediments were first carried by the Yellow River from the NTP to the floodplain northwest of the Mu Us Desert (Yinchuan-Hetao Graben), and were then entrained by near-surface winds to the downwind CLP (Stevens et al., 2013; Nie et al., 2015). Studies on the sedimentology of a loess-palaeosol sequence in the Mangshan Loess Plateau (MLP) in the lower reach of the Yellow River indicate that the Yellow River floodplain has been the main dust source of the aeolian loess deposits in the southeastern part of the CLP during the last glacial-interglacial cycle (Zheng et al., 2007; Prins et al., 2009). However, no diagnostic provenance evidence is currently available for this. The MLP is located just downwind of the Yellow River floodplain and near the boundary of the middle and lower reaches of the Yellow River (Fig.1.1). Reconstruction of the dust supply history of the loess-palaeosol sequence in the MLP would provide a case study to examine the role of the Yellow River in transporting sediments to the aeolian deposits in the CLP and further help us to understand the developmental history of the drainage system of the Yellow River.

While numerous studies have focused on the provenance analysis of Quaternary loess-palaeosol sequences, the sediment source(s) for the late Neogene Red Clay deposits are less well studied and understood. Nie et al. (2014) provided the first provenance data based on the zircon U-Pb age components for the Red Clay sequence in the central CLP, and their results revealed multiple sources for these deposits: dust generated from the Taklimakan Desert by westerly winds is the dominant source for the early Pliocene Red Clay, whereas late Pliocene Red Clay is similar to the source of the Quaternary loess, and was mainly derived from the NTP. However, it is still unclear whether the source, or sources, of the Red Clay is spatially variable due to a paucity of available provenance data. Detailed and systematic provenance work on multiple Red Clay sites across the CLP was needed to better constrain the source areas and the transport pathways of the Red Clay and thus the wind patterns responsible for dust delivery during the Late Neogene.

1.2. Study area, studied sites and collected material

1.2.1. Chinese Loess Plateau

The Chinese Loess Plateau (CLP), with an elevation varying between 800 and 3000 metres, extends from 32°N to 40°N and from 98°E to 115°E, covering about 600,000 km^2 in northern China (Liu, 1999). It largely overlaps with the upper and middle reaches of the Yellow River drainage area and is bounded by the Mu Us Desert to the north, the Qinling Mountains to the south, the Helan Mountains to the northwest, the Qilian Mountains to the west and the Taihang Mountains to the east (Fig.1.2). The climate in this area is highly seasonal and monsoon influenced: in winter, the stable Siberian-Mongolia anticyclone results in a cold and dry air flow coming from the north and the northwest known as the East Asian winter monsoon, while in summer, moisture is brought to the continent by the warm air flow from the ocean in the south and southeast, known as the

East Asian summer monsoon. The mean annual temperature in the region increases from 4 °C in the northern CLP to 14 °C the southern CLP, and the mean annual precipitation rises from less than 200 mm in the northwest to 650 mm in the southeastern CLP (UCAR, 2006). Along this climatic gradient, the modern vegetation cover changes from

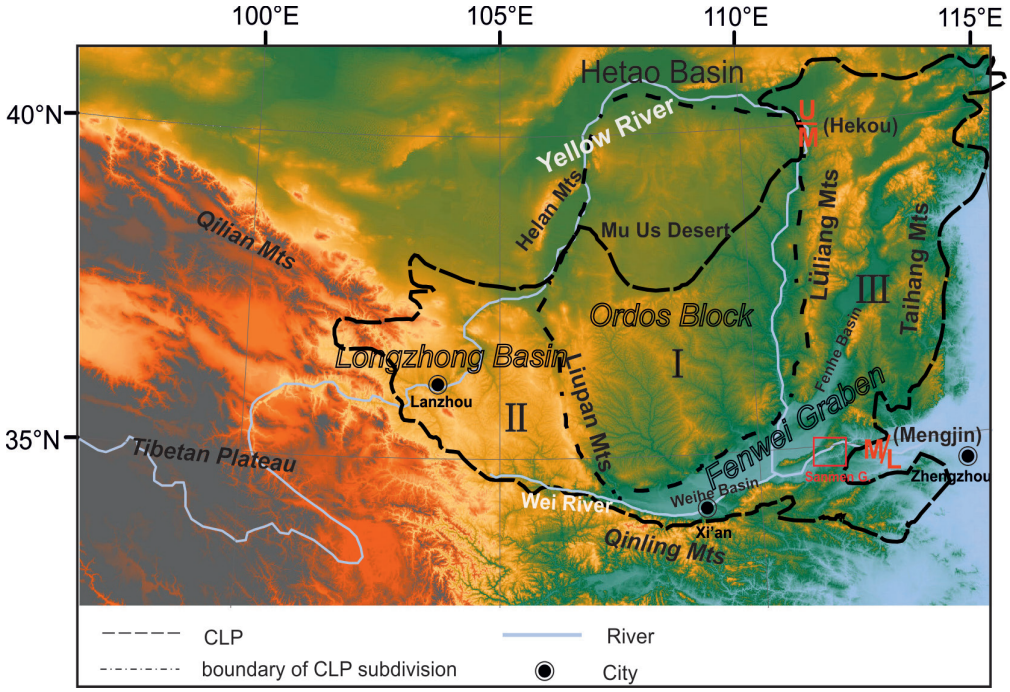

Figure 1.2. The Chinese Loess Plateau and three subdivisions. I, the Ordos Block ; II, the Longzhong Basin and III, the Fenwei Graben. The red letters indicate the boundaries between the upper and middle reach and the middle and lower reaches of the Yellow River. The red rectangle marks the location of the Sanmen Gorge. The figure is modified after Yuan et al. (2012).

arid steppe to forest steppe and finally to broadleaved forest in a southeastern direction.

The CLP is famous for its characteristic loess landscapes and continuous Neogene and Quaternary dust records. According to the tectonic setting and loess landscapes, the CLP can be grouped into three regions: I) the Ordos Block, II) the Longzhong Basin and III) the Fenwei Graben (Yuan et al., 2012).

The central CLP lies within the body of the Ordos Block. The Ordos block is rimmed by the Hetao Basin to the north, the Liupan Mountains to the west, the Weihe Basin to the south and the Lüliang Mountains to the east. During the early Cenozoic there was tectonic quiescence; the area suffered extensive erosion, which resulted in the formation of a gentle-sloped planation surface (Yuan et al., 2012; Nie et al., 2016). During the late Cenozoic, due to the India-Asian collision and uplift of the Liupan Mountains, the planation surface was disrupted and the area was dissected into a maze of gullies and hills. Three main loess landform types are distinguished in the area: plateau or tableland (called Yuan in Chinese), elongated ridges (Liang) and hemispherical hills (Mao) (Liu, 1985). The most complete Neogene-Quaternary aeolian records are found within this region, where the Quaternary loess deposits conformably overlie the late Miocene-

Pliocene Red Clay. The continuous loess-palaeosol sequences found in the central CLP consist of 33 palaeosol and 34 loess units with a depositional age spanning from ~2.6 to 0 Ma (Liu et al., 1999). Most Red Clay sequences in the Ordos Block have a basal age of ~7–8 Ma (Sun et al., 1998a; Ding et al., 2001b; Qiang et al., 2005).

The Longzhong Basin is located west of the Liupan Mountains and its western and southwestern borders extend to the Northern Tibetan Plateau (NTP). It is a Cenozoic foreland basin resulting from the India–Asian collision (Horton et al., 2004). This region is characterised by the Red Clay landform of Neogene age, covered with a thin loess layer. Exceptionally thick loess successions of up to 300 m are found in the Lanzhou area (Liu, 1985; An et al., 2001; Yuan et al., 2012). Aeolian dust deposition in this region started at least 22 Ma (Guo et al., 2001); a recent study extended the basal age of the sequence back as far as 25 Ma (Qiang et al., 2011).

The Fenwei Graben of the eastern CLP is a crescent-shaped rift valley bordered by the Ordos Block to the west, the Qinling Mountains to the south and the Taihang Mountains to the east. It is comprised of two sub-basins: the Weihe Basin in the southwest and the Fenhe Basin in the north and northeast, covering an area of more than 20,000 km^2. This graben experienced continuous subsidence during the Eocene due to the eastward extrusion of the Tibetan Plateau and has been filled by remarkably thick deposits (Liu et al., 1960; Zhang et al., 1978; AFSOM, 1988; Hu et al., 2016; Rits et al., 2017). Thick lacustrine sediments indicate that there was a large palaeolake (Sanmen Lake) in the Weihe Basin extending from the Sanmen Gorge westwards to Baoji (AFSOM, 1988; Kong et al., 2014). It has been suggested that the lake was drained due to the incision of the Yellow River through the Sanmen Gorge (Wang, 2002; Yuan et al., 2012; Kong et al., 2014). In the Fenwei Graben, Quaternary loess deposits overlie the lacustrine sediments or river terraces, forming the yuan tableland loess landscape. Here Red Clay sequences are sporadically found. Two typical and well-studied Red Clay sites are the Lantian site in the southwest corner of the Weihe Basin (Kaakinen and Lunkka, 2003; Zhang et al., 2013b) and the Yushe site on the eastern flank of the Lüliang Mountains (Flynn et al., 2011; Tedford et al., 2013; Flynn and Wu, 2017).

1.2.2. Yellow River

With a total length of 5500 km, the Yellow River (Huanghe) is one of the largest rivers of the world. It originates from the northern Tibetan Plateau and has deeply incised into a series of intermontane basins and bedrock ranges along the northeastern plateau margin. After a 1500 km-long U-bend developed around the Ordos Block, it runs through the Sanmen Gorge and flows onto a wide floodplain in the low-gradient eastern part of China (North China Plain) and eventually discharges into the Bohai Sea (Fig. 1). Traditionally, the river has been divided into an upper, a middle and a lower reach. The boundary between the upper and middle reaches is located near Hekou town on the northeastern edge of the Ordos Block, while transition between the middle and lower reaches is located at Mengjin near the Mangshan Loess Plateau. Since the Yellow River flows through the CLP, which is subject to high erosion rates, it is currently one of the most sediment-laden rivers in the world. It has been proposed that the integration of the modern Yellow River

is a consequence of cutting through of a series of isolated inland fluvial-lacustrine basins by headward erosion (Craddock et al., 2010). However, the geological history of the Yellow River, particularly for its middle and lower reaches is still largely debated and the suggested timing for the fully incision of the Yellow River through the Sanmen Gorge varies from the late Miocene to the Pleistocene (Lin et al., 2001; Wang, 2002; Craddock et al., 2010; Wang et al., 2013; Kong et al., 2014; Hu et al., 2017).

1.2.3. Red Clay sites

In this study, three Red Clay sites (Baode, Lantian and Dongwan; see Fig. 1.3, 1.4)

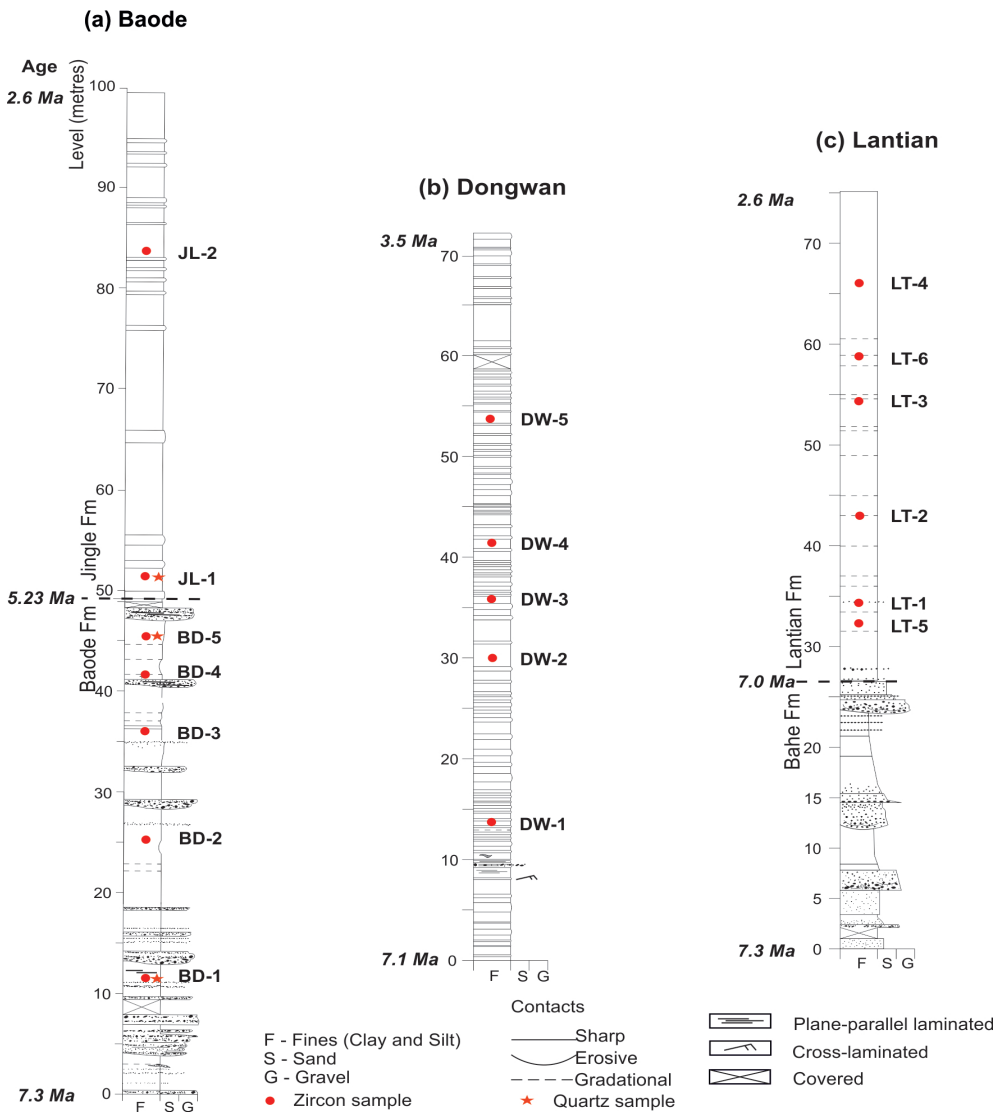

Figure 1.3. Lithology of the studied Red Clay sites **(a)** Baode (Jingle), **(b)** Dongwan and **(c)** Lantian. Red dots and red stars mark the levels of samples collected for zircon U-Pb dating and *in situ* quartz trace elements analysis, respectively. The samples for dynamic image analysis of grain size and shape are not marked here, but are shown in Fig. S1 in Chapter 4.

representing a variety of geographical and local sedimentary settings across the CLP were investigated.

The Baode site in the northeastern CLP is surrounded by the Lüliang Mountains to the east and the Yellow River to the west (Fig.1). Baode is an area where the "*Hipparion* fauna" in northern China was discovered and the term "*Hipparion* Red Clay" was then established by Zdansky (1923) to define the fossiliferous Red Clay deposits in the area. The late Neogene Red Clay and Quaternary loess-palaeosol strata are exposed in steeply sloping gullies and ravines and rest on the Palaeozoic basement with an angular unconformity. The late Neogene stratigraphy of Baode has been grouped into two formations: the Baode and Jingle Formation (Fm) (Teilhard de Chardin and Young, 1931; Zhu et al., 2008; Kaakinen et al., 2013). The underlying Baode Fm is typically about 60 m thick and contains abundant mammalian fossils of late Miocene age. It has a more variable lithology compared to the overlying Jingle Fm. The lower part of the Baode Fm has abundant conglomerates of varying thickness, whilst the upper part, representing the bulk of the Baode Fm, is composed of red brown clays and silts with alternating carbonate nodule-rich horizons and infrequent sheet conglomerate beds. The Jingle Fm is up to ca. 40 m thick and conformably overlies the Baode Fm. It is exclusively composed of clay and silt-sized lithologies with a distinctive deep red colour and is devoid of sand and gravel lithologies. Carbonate-rich horizons and abundant Fe-Mn coating present in the deposits indicate strong pedogenesis of the soil.

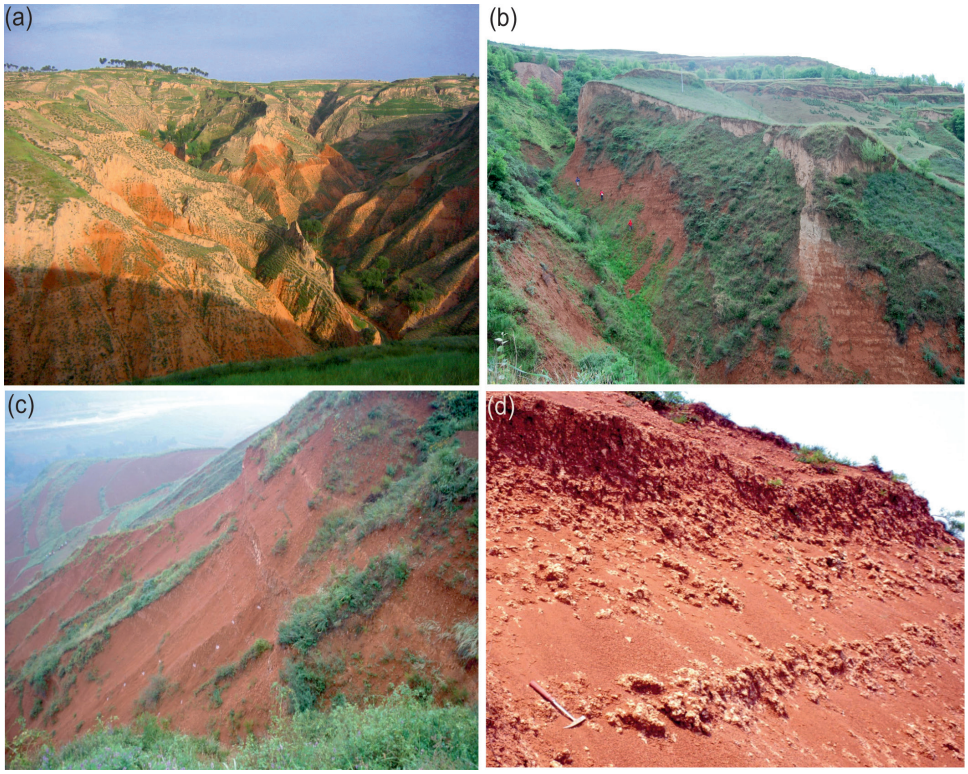

Figure 1.4. The studied Red Clay sites of **(a)** Baode, **(b)** Dongwan and **(c)** Lantian and **(d)** the carbonate nodule rich horizon of the Lantian Fm. Photos by Anu Kaakinen.

Magnetostratigraphic dating has assigned a basal age of 7.23 Ma to the Baode Fm and a depositional age of 5.23 to 2.72Ma to the Jingle Fm (Zhu et al., 2008; Kaakinen et al., 2013).

The Lantian site in the southernmost CLP is located in the foothills of the northern flank of the Qinling Mountains, within the southeastern Weihe Basin. It comprises of a thick accumulation of Cenozoic clastic sediments (Kaakinen, 2005). The late Neogene sediments in this area include the Lantian Fm and the underlying Bahe Fm. With a thickness of 280m, the Bahe Fm is mainly composed of fluvial deposits characterised by thick and laterally continuous floodplain deposits (Kaakinen and Lunkka, 2003; Zhang et al., 2013b). Based on geochemical and grain-size evidence, these fine-grained units have been suggested to be partly aeolian (Wang et al., 2014). The overlying the Lantian Fm is a Red Clay succession comprising distinctive deep-red fine-grained deposits with cyclic carbonate nodule-rich horizons progressively becoming more abundant in the upper part of the formation (Fig. 1.4c, d). As demonstrated by magnetostratigraphic dating studies (Kaakinen, 2005; Wang et al., 2014; Zhang et al., 2013b) the basal age for the Bahe Fm is at ca. 11 Ma and the boundary between the Bahe and Lantian Fm is ca.7 Ma.

The Dongwan Red Clay succession in the western CLP represents the loessic Red Clay deposits in the west of the Liupan Mountains (Fig. 1.1). It is characterised by a 74-m-thick sequence of dominantly massive reddish silt beds and carbonate rich couplets, with thin laminations indicating water-lain settling recognized in the lower part of the sequence (Fig. 1.3). Fossil micromammals (Liu et al., 2011; Liu et al., 2013) and terrestrial molluscs (Li et al., 2014) are present throughout the sequence. Compared to the Red Clays of Baode and Lantian, relatively weaker nodule formation is shown in the carbonate units in Dongwan. According to Hao and Guo (2004), the Dongwan Red Clay succession is dated to the time interval of 7.1 to 3.52 Ma based on magnetostratigraphy.

Samples were taken from the fine-grained lithologies. For the Baode Fm and lower part of the Lantian Fm, where conglomerates or sandstones are shown, laterally equivalent fine-grained facies was sampled, when possible. The sampling levels for zircon U-Pb dating and for the analysis of the trace element content in quartz analysis are indicated in Figure 1.3.

1.2.4. Loess –palaeosol sequences

To characterise the transport pathways of loess across the central CLP, four loess-palaeosol sections located along a transect oriented north-to-south oriented across the main body of the CLP, Huanxian (HX), Xifeng (XF), Xunyi (XY) and Duanjiapo (DJP), were selected and sampled for grain size and shape analysis (Fig. 1.1). Detailed descriptions and age models of the sections are presented in Nugteren and Vandenberghe (2004) and Prins and Vriend (2007). All the sections cover the last two glacial and interglacial cycles (S0–L1–S1–L2–S2), except the DJP sequence in the southernmost CLP, which comprises the last glacial–interglacial period (S0-L1) (Fig. 1.5). Samples from the same stratigraphic intervals representative for the typical loess (glacial and stadial loess L1-1,

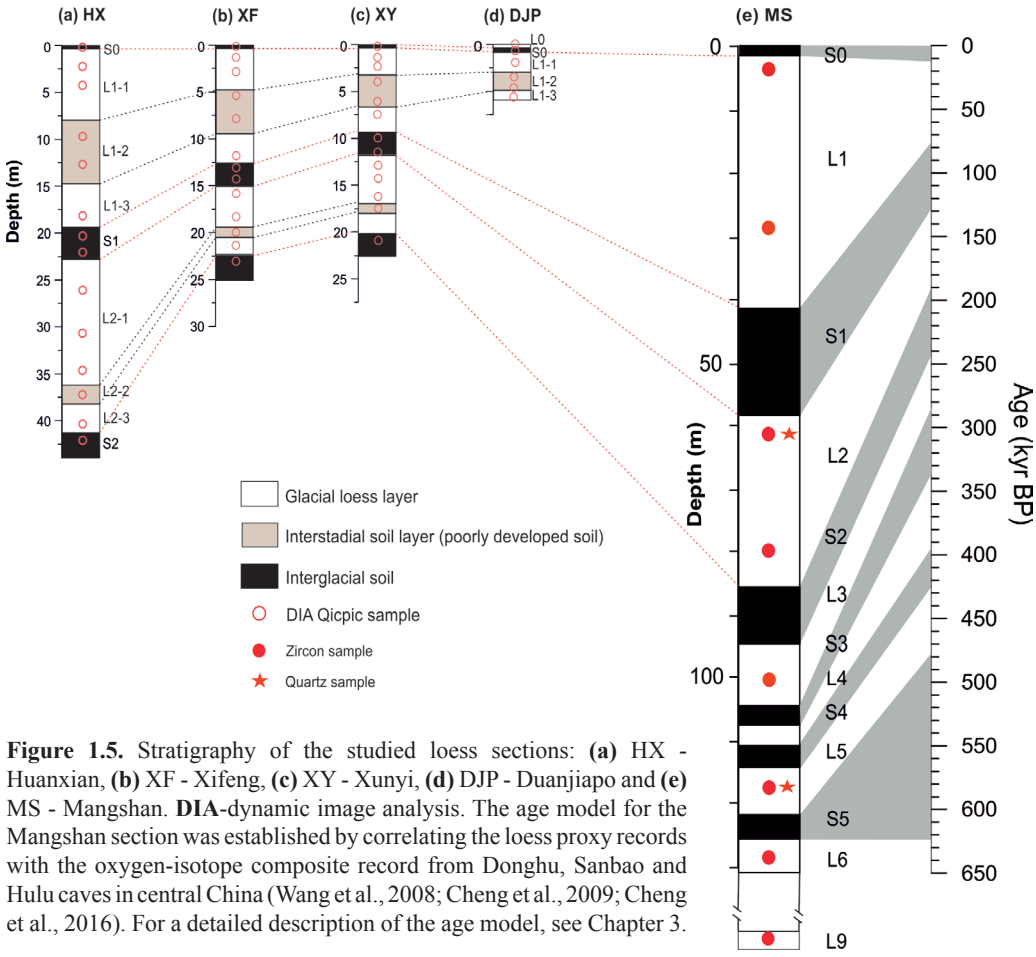

Figure 1.5. Stratigraphy of the studied loess sections: **(a)** HX - Huanxian, **(b)** XF - Xifeng, **(c)** XY - Xunyi, **(d)** DJP - Duanjiapo and **(e)** MS - Mangshan. **DIA**-dynamic image analysis. The age model for the Mangshan section was established by correlating the loess proxy records with the oxygen-isotope composite record from Donghu, Sanbao and Hulu caves in central China (Wang et al., 2008; Cheng et al., 2009; Cheng et al., 2016). For a detailed description of the age model, see Chapter 3.

L1-3, L2-1 and L2-3), well-developed soil (interglacial palaeosol, S1 and S2) and poorly developed soil (interstadial palaeosol, L1-2 and L2-2) units of individual loess sections were collected (Fig. 1.5).

In this work (Chapter 3), a detailed study of the sedimentology and provenance of the loess-palaeosol sequence from the Mangshan Loess Plateau (MLP) was carried out. Mangshan is located near the boundary of the middle and lower reaches of the Yellow River (Fig. 1.1), and in the topographic transition border between the uplifting region in the west and subsiding region in the east. About 200 km upstream, the Yellow River cuts through the Sanmen Gorge, initially releasing a tremendous silt load from the CLP. This results in the formation of a large fluvial-alluvial fan east of the gorge, which constitutes the southwestern part of the North China Plain (NCP). Downstream, the Yellow River gradually flows through the NCP with a low gradient and eventually discharges into the Bohai Sea. Typical loess-palaeosol successions are well exposed on the northern slope of the MLP, where the Yellow River has laterally cut the plateau and formed a deep scarp along its northern edge (Fig.1.6). Field observations have identified 11 loess units and 12 palaeosol units for the exposed Mangshan loess deposits (Ji et al., 2004; Zheng et al.,

2007; Qiu and Zhou, 2015). The studied section of this work with a total thickness of 171 m, is located near the village of Liugou about 25 km northwest of Zhengzhou city. The magnetostratigraphy has been established by Zheng et al. (2007), setting the Brunhes/Matuyama (B/M) boundary at a depth of about 150 m in the lower part of loess unit L8 in the section, demonstrating the resemblance between the Mangshan loess sequence and the other typical loess-palaeosol sequences found on the CLP. The upper part of the sequence (upper 100 m, above palaeosol S2) (Fig.1.5) is characterised by higher

Figure 1.6. Mangshan Loess Plateau (MLP) in the lower reach of the Yellow River. Photo by Yuan Shang.

sedimentation rates and coarser-grained loess sediments compared to the lower part of the sequence and the loess deposits in the central CLP (Zhang et al., 2004; Zheng et al., 2007; Prins et al., 2009; Qiu and Zhou, 2015). In this study, the main focus was on the upper 130 m of the Mangshan Plateau sequence, which covers palaeosol unit S0 to loess unit L6, with an additional (zircon) sample taken from loess unit L9.

1.3. Objectives of the study

The main aim of this (PhD) study was to provide a comprehensive approach to examine the long-term dust supply and transport patterns developing during the late Neogene and Quaternary in the CLP of northern China, and their response to changes in climate and tectonic evolution. To this end, a combination of both conventional and novel sedimentological and provenance analytical methods was used.

The specific objectives were:

1) To provide a detailed provenance analysis based on the zircon U-Pb ages for the late Miocene-Pliocene Red Clay sequences to investigate the spatial and temporal variations in the sources of the Red Clay, and to subsequently investigate the dust

transport pathways and prevailing wind patterns during the late Neogene by dust trajectory modelling (Chapter 2);

2) To investigate the role of the Yellow River in supplying dust to the Quaternary loess deposits and study the mechanisms that control the sedimentology and provenance changes of the loess-palaeosol sequences (Chapter 3);

3) To examine the subpopulations and their relative proportions in the bulk Red Clay and loess deposits by applying an end-member modelling approach to an extensive grain size dataset. The aims were to understand the dust transport process related to each subpopulation and examine the (dis-) similarity of the transport and depositional processes between Red Clay and loess deposits (Chapters 2 and 3);

4) To determine the dust transport pathways and reveal the aeolian sorting pattern by applying dynamic image analysis (DIA) to characterise the grain size and shape distribution of the silt and fine sandy particles of the loess and Red Clay deposits (Chapter 4);

5) To test the application of the trace element content in quartz grains as an alternative

Table 1. Description of the studied Red Clay and loess sections and related methods

Sites	Late Miocene-Pliocene Red Clay			Quaternary loess				
	Baode (Jingle)	**Lantian**	**Dongwan**	**Mangshan**	**Huanxian**	**Xifeng**	**Xunyi**	**Duanjiapo**
Coordinates	38.99°N 111.14°E	34.25°N 109.12°E	34.96°N 105.78°E	34.95°N 113.37°E	36.6°N 107.3°E	35.88°N 107.97°E	35.06°N 108.3°E	34.2°N 109.4°E
Studied age interval	7.23 – 3.5 Ma	5.83 – 3.7 Ma	6.73 – 4.36 Ma	900 ka – 0 (L9–S0)	225 ka – 0 (S2–S0)	225 ka – 0 (S2–S0)	225 ka – 0 (S2–S0)	70 ka – 0 (L1–S0)
Sample analysis	Grain size (LD, DIA) Grain shape (DIA) Zircon U-Pb Quartz trace elements	Grain size (LD, DIA) Grain shape (DIA) Zircon U-Pb	Grain size (LD, DIA) Grain shape (DIA) Zircon U-Pb	Grain size (LD) Zircon U-Pb Quartz trace elements Carbonate content Organic content	Grain size (LD, DIA) Grain shape (DIA)	Grain size (LD, DIA) Grain shape (DIA)	Grain size (LD, DIA) Grain shape (DIA)	Grain size (LD, DIA) Grain shape (DIA)
Statistical analysis	EMMA MDS	EMMA MDS	EMMA MDS	EMMA MDS	EMMA	EMMA	EMMA	EMMA
Climate modelling	Dust trajectory modelling	Dust trajectory modelling	Dust trajectory modelling					
Chapter	2, 4, 5	2, 4	2, 4	3, 5	4	4	4	4

tool to determine the dust source of the aeolian loess and Red Clay deposits (Chapter 5).

1.4 Study Methods

The analysis conducted for each of the studied sites is summarised in Table 1.

1.4.1. Grain size and shape analysis

Grain size analysis was performed for Red Clay and loess samples in Chapters 2, 3 and 4. Following the standard analytical procedure for loess and Red Clay (cf. Konert and Vandenberghe, 1997; Vandenberghe et al., 2004), about 0.5–1.0 g of bulk sediment was pre-treated with H_2O_2 and HCl to remove organic matter and carbonates, respectively. The grain-size records of the loess sections Huanxian, Xifeng, Xunyi, Duanjiapo and Mangshan, and of the Red Clay section of Lantian were obtained using a Fritsch A22 laser-diffraction (LD) instrument at Vrije Universiteit Amsterdam (VUA). Red clay samples from the Jingle Fm of Baode and from Dongwan were analysed using a Sympatecs KR laser-diffraction particle sizer at VUA. Red Clay samples of the Baode Fm were analysed using a Coulter LS200 at the University of Helsinki (UH). All the LD devices used in this study produce grain-size distributions with 56 size intervals within the size range 0.15–2000 μm. We used the GRADISTAT program developed by Blott and Pye (2001) to calculate the median grain sizes of the samples.

The image analysis sensor Qicpic/R (http://www.sympatec.com/EN/ImageAnalysis/QICPIC.html) developed by Sympatec was used in Chapter 4 to characterise the grain size and shape of silt and fine sandy particles in the loess and Red Clay deposits. This was the first time that dynamic image analysis (DIA) had been applied to Chinese aeolian dust. The pre-treatment of the Red Clay and loess samples for DIA followed the same procedure as the LD grain-size analysis to ensure that the particles were well dispersed during measurement. DIA provides information of the size and shape of a particle based on a 2D image of the particle's contour. In this study, the mean Feret diameter and aspect ratio were used to describe the size and shape of a particle, respectively. Additionally, silty and sandy size fractions expressed as parts per million (ppm) of the total number of particles analysed (bulk sample) were calculated for the Red Clay and loess samples in order to investigate the grain-size components of bulk sediments. The particle counts of the >32 μm, >63 μm, >125 μm and >250 μm fractions were reported and included for detailed analysis.

1.4.2. Zircon U-Pb dating

Detrital zircon U-Pb dating was used to characterise the provenance of the Red Clay and loess deposits in Chapters 2 and 3. Separation of the zircon grains from the bulk samples was conducted at the Mineral Separation Laboratory of VUA. About 0.5–5.0 kg bulk sediments was wet-sieved over a 20-micron sieve and treated with 5% HCl to remove carbonate. Zircon grains were collected after heavy liquid (density of 2.86 and 3.30 g/cm^3 LST heavy liquid) and Frantz magnetic separation. Zircon grains were handpicked and mounted in a 2.5-cm-diameter epoxy resin disc, sectioned approximately in half and polished. In addition, photomicrographs of zircons were taken with an Olympus stereo

zoom microscope for zircon morphology analysis before mounting and polishing. Back-scattered electron images (BSE) were prepared for the zircons to target the spot sites.

Detrital zircon U-Pb ages were determined by laser-ablation-inductively coupled plasma-mass spectrometry (LA-ICP-MS) at the Finnish Geosciences Research Laboratory, Geological Survey of Finland, in Espoo. Red Clay samples of Lantian, Dongwan and Baode were analysed with a Photon Machine Analyte G2 laser microprobe using a similar technique as in Rosa et al. (2009). The loess samples and fluvial samples were analysed by a Nu Plasma AttoM single collector ICPMS connected to a Photon Machine Excite laser ablation system. Typical ablation conditions included a beam diameter of 20–29 μm, a pulse frequency of 5 Hz and a beam energy density of 2 J/cm^2. The calibration standard GJ-1 (609 ± 1 Ma) (Belousova, 2005) and in-house standards A382 (1877 ± 2 Ma) and A1772 (2712 ± 1 Ma) (Huhma et al., 2012) were run at the beginning and end of each analytical session, and at regular intervals during sessions. The Glitter program was used for calibration of the raw data (Van Achterbergh et al., 2001). All the ages were calculated with 2σ errors and without decay constants errors. The $^{207}Pb/^{206}Pb$ age offset from concordant ID-TIMS ages for several samples did not exceed 0.5%. We used $^{238}U/^{206}Pb$ ages for ages younger than 1Ga and $^{207}Pb/^{206}Pb$ ages for ages older than 1 Ga. Ages were rejected if discordance exceeded ±15% for Red Clay and ±10% for loess and fluvial sands.

1.4.3. Trace elements content in quartz

In Chapter 5, we explored the possibility of using the trace elements content in quartz as a provenance tool for the loess and Red Clay deposits. The preparation work required thorough cleaning of the quartz grains in order to remove clay minerals and other potential contamination attached to the surface of the quartz. The trace element concentration in quartz was measured with an Agilent 7900s ICP Mass spectrometer coupled with a Coherent GeoLas Pro MV 193 nm excimer laser-ablation system at the Department of Geosciences and Geography, University of Helsinki. The detailed set-up for the measurement is presented in Chapter 5. The instrument accuracies of 39 elements were monitored daily by measuring the composition of NISTSRM612 synthetic glass standards using NISTSRM610 as the external standard. The measurements were accepted if the concentrations were within 5% of the preferred values and the propagated uncertainties associated with NISTSRM610 and NISTSRM612 (Spandler et al., 2011). The following trace elements were included in the mass scan table: ^{7}Li, ^{11}B, ^{23}Na, Mg^{25}, ^{27}Al, ^{31}P, ^{34}S, ^{35}Cl, ^{39}K, ^{42}Ca, ^{45}Sc, ^{47}Ti, ^{49}Ti, ^{55}Mn, ^{57}Fe, ^{65}Cu, ^{66}Zn, ^{71}Ga, ^{72}Ge, ^{85}Rb, ^{88}Sr, ^{90}Zr, ^{133}Cs, ^{137}Ba, ^{208}Pb and ^{238}U. However, only ^{7}Li, ^{45}Sc and ^{49}Ti were found to consistently be suitable for application as provenance tracers. The energy density was 10 J/cm² for standard NISTSRM610 and 14 J/cm² for quartz. For each analysis, the repetition rate was 10 Hz and the dwell time per isotope was 10 ms. Laser spot sizes from 30~90 μm were used, depending on the grain size of the quartz.

1.4.4. End member modelling of grains-size distributions

Sediment fluxes from multiple sources and transporting patterns can be detected by means of end-member modelling of the grain size distribution (Stuut et al., 2002; Weltje and Prins, 2003; Weltje and Prins, 2007). It has been well used in distinguishing aeolian from

fluvial input in various marine settings (Prins et al., 2000; Stuut et al., 2002; Deplazes et al., 2014; Stuut et al., 2014). Previous studies have also suggested that a genetically meaningful unmixing of loess grain size distributions can be accomplished with an end-member modelling algorithm (EMMA) (Vriend and Prins, 2005; Prins and Vriend, 2007; Prins et al., 2009; Vriend et al., 2011). In this work, we applied the EMMA to the grain-size distributions of both the Quaternary loess-palaeosol sequences (Chapter 3 and Chapter 4) and late Miocene-Pliocene Red Clay sequences (Chapter 2, 4) to characterise the subpopulations of the mixed aeolian sediments (and their relative contribution within the sections) and to distinguish the possible fluvial input in the Red Clay deposits.

End-member modelling consists of two stages: in the first stage the numbers of end members (EMs) are estimated according to the mean coefficient of determination (r^2), and in the second stage, the proportions of each EM are calculated. The coefficient of determination (r^2) represents the proportion of the variance of each grain size reproduced by the approximated data (Weltje, 1997). The mixing model is chosen when the r^2 shows a satisfactory goodness of fit (usually >0.8). This means that the selected model provides a good description of the variation in the grain-size distribution dataset.

1.4.5. Visualisation of zircon U-Pb data and the multi-mimensional scaling (MDS) map

Probability density plots (PDP; Ludwig, 2003), kernel density estimation (KDE, Vermeesch, 2012) plots and histogram diagrams have been used to visualise the zircon age distributions of Red Clay and loess samples. Zircon grains from different stratigraphic units are combined within the section in order to better assess the difference between individual sites and to reduce the bias and statistical errors brought about by (too) small sample sizes. A non-metric multi-dimensional scaling (MDS) map (Vermeesch, 2013) was employed to visualise the (dis) similarities between the combined large zircon datasets of Red Clay, loess and the sediments of potential source areas. This technique works in a similar way to principal component analysis which is able to capture the main feature of the detrital zircon age datasets and has been well practiced in previous provenance studies on Red Clay and loess (Che and Li, 2013; Stevens et al., 2013; Vermeesch, 2013; Nie et al., 2014; Bird et al., 2015). We also used the MDS map for visualising a comparison of trace element contents in quartz from the Red Clay, loess and desert sands samples.

1.4.6. Dust trajectory modelling

The trajectory model HYSPLIT version 4 (Draxler and Hess, 1998) was employed to simulate the potential transport paths of the aeolian deposit in the three Red Clay sections during the late Miocene. The output from a Late Miocene global model simulation by Micheels et al. (2011) was used as the meteorological data to drive HYSPLIT. Three-dimensional 5-day backtrace trajectories of the near surface air mass (1000 m above ground level) of the three Red Clay localities were calculated every 12 hours for both winter (December, January, February) and spring (March, April, May). Finally, all the calculated trajectories were grouped into 4–5 mean trajectories to represent the dominant pathways of the air mass delivering dust to the studied Red Clay localities.

1.5. Outline of the thesis

This thesis is comprised of six chapters. Chapter 1 is a general introduction of the thesis. Chapter 2 to 5 are based on four peer reviewed scientific publications and Chapter 6 is a synthesis, which summarises the major results and implications of this work.

Chapter 2 investigated the spatiotemporal variations in the provenance of late Miocene-Pliocene Red Clay of the CLP. Three well-known Red Clay sequences in the CLP: Baode in the northeast, Lantian in the south and Dongwan in the west were examined. Firstly, an end-member modelling approach was applied to the grain-size distribution dataset of the three Red Clay sequences to characterise the subpopulations of the sediments and their relative contributions within the sections and to understand the corresponding transport and depositional processes for the various components (Fig. 3 in Chapter 2). Subsequently, single grain zircon U-Pb dating was used to explore the potential sources for the Red Clay (Fig. 4 and Fig. 5 in Chapter 2). Additionally, backtrace trajectory modelling was employed to investigate the transport pathways of the studied Red Clay localities and the prevailing wind patterns over the CLP in the late Miocene and Pliocene (Fig. 7 in Chapter 2). It was revealed that the clay dominated Red Clay of the southern (Lantian) and western (Dongwan) CLP was mainly derived from the Northern Tibetan Plateau (NTP) and Taklimakan Desert and was delivered by low level westerly winds. The more silt-dominated Red Clay in the northeastern CLP (Baode) is comprised of sediments transported from the NTP and a broad area of northern China (Central China Orogenic Belt) by northwesterly and northerly winds. The results are comparable to the dust supply pattern of the Quaternary loess, implying that a consistent spatial pattern variation in the provenance of the wind-blown sediments in the CLP started at least since the late Miocene. Temporally, Baode Red Clay in the NE CLP shows an increased source signature from the western deserts since 3.6 Ma. This might have resulted from the uplift of the Tibetan Plateau and Tianshan Mountains in the Pliocene, which intensified the westerly wind strength and/or aridity of western China. This could also be connected with the onset of enhanced drainage of the Yellow River promoted by increased denudation of the NTP since 3.6 Ma which allowed more sediments to be delivered to the CLP by the Yellow River.

Chapter 3 studied the role of the Yellow River in supplying dust to the loess deposits and the mechanism behind the change in sedimentology of the loess-palaeosol sequence from the Mangshan Loess Plateau (MLP) along the lower reach of the Yellow River (Fig. 1 in Chapter 3). The sub-components of the Mangshan loess and its contributions within the bulk sediments were characterised by an end-member modelling approach applied to a grain size distribution dataset (Fig. 2 and Fig.3 in Chapter 3). A dust flux model was used to investigate the change in the dust accumulation rate along the sequence (Fig. 4 in Chapter 3). Fingerprinting of the source of Mangshan loess and its provenance variation was achieved by mean of single grain zircon U-Pb dating (Fig. 5 and Fig.6 in Chapter 3). The similarity of zircon U-Pb age components between the Mangshan loess and the Yellow River sediment suggests that loess deposits of the MLP have mainly been derived from the Yellow River floodplain north of the plateau. No obvious temporal variation has been found in the provenance signal of the Mangshan loess from loess units L9 to L1,

indicating that the dust supply from the Yellow River floodplain to the MLP was initiated at least 900 ka (MIS22). This implies that the Yellow River cut though the Sanmen Gorge at least before 900 ka. Grain-size data and the dust flux model show that both the coarser-grained fraction and the dust accumulation rate have significantly increased in the upper Mangshan loess sequence above S2, suggesting increased sediments supply and a more proximal source to MLP since 240 ka. The sudden change in sedimentology (grain size and accumulation rate) of the Mangshan loess around 240 ka is contemporaneous with tectonic movements in the Weihe Basin. This probably suggests that due to tectonic uplift in the Weihe Basin around 240 ka, rapid fluvial incision in the basin caused tremendous amount of fluvial sediments to be carried out of the Sanmen Gorge to the lower reach of the Yellow River, leading to the formation of a larger fluvial fan north of the MLP and resulting in increased dust being transported to MLP via aeolian processes. Moreover, the southern migration of the Yellow River evidenced by a northern high scarp of the MLP probably provided a more proximal source area for the MLP during the middle and late Pleistocene.

Chapter 4 aimed to fingerprint the transport process of the silt (2–63 μm) particles in the late Neogene and Quaternary aeolian sediments (Red Clay and loess) of the CLP by applying dynamic image analysis (DIA; Sympatec Qicpic) in the characterisation of the grain-size and grain-shape distribution. Samples were collected from four Quaternary loess sections, namely Huanxian, Xifeng, Xunyi and Duanjiapo, along a north-to-south transect in the CLP and from three Red Clay sequences distributed across the CLP: Baode in the northeast, Lantian in the south and Dongwan in the west (Fig. 1 in Chapter 4). The grain-size distribution of the samples was measured both by DIA and laser diffraction (LD) particle size analysis (Fig.4 in Chapter 4). Similarly to the grain size dataset produced by LD, DIA characterisation of grain-size distribution of Quaternary loess not only differentiated the glacial loess units from interglacial palaeosol units but also revealed clear spatial variation, with the grain size decreasing from the northern to the central and to the southern parts of the CLP during the last two glacial and interglacial cycles (Fig. 6 and Fig. 7 in Chapter 4). A similar spatial pattern is also revealed by the DIA on the fine-grained Miocene-Pliocene Red Clay (Fig. 8 in Chapter 4). Moreover, DIA was able to characterise the fluvial contribution to the Red Clay, as indicated by different grain-size and grain-shape distributing curves (Fig. 9 in Chapter 4). The grain-shape analysis of DIA revealed a systematic pattern for both the loess-palaeosol sequences and Red Clay sediments, whereby the aspect ratio decreased as a function of increasing grain size (Fig. 7 and Fig. 9 in Chapter 4). This probably suggests that systematic shape sorting occurred during the aeolian transportation of the silt particles. We found that certain grain size ranges corresponded to specific aspect ratios that seemed to be aerodynamically distinguishable from each other and that could be further linked to the wind velocity/strength in transporting the particles.

Chapter 5 introduced a new approach for characterising the provenance of detrital quartz from the loess and Red Clay deposits by using laser-ablation inductively coupled plasma-mass spectrometry (ICP-MS). Trace elements in quartz were analysed from Quaternary loess samples of the Mangshan Plateau in central China, late Miocene-Pliocene Red Clay samples of the Baode section in the northeast of the Chinese Loess

Plateau and sand dune samples from the major deserts in northern and western China (Fig. 1in Chapter 5). Three trace elements (Li, Ti and Sc) in quartz are presented (Fig. 3 in Chapter 5) and the data indicate that the Qaidam Basin has a similar trace element distribution in quartz to that in Quaternary loess, implying a significant contribution of debris from the Qaidam Basin to the loess deposits in the northern China (Fig. 4 in Chapter 5). The data also suggest a possible dust supply from the Taklimakan Desert to the Baode Red Clay, as demonstrated by the similarity of the Ti and Sc contents in the quartz grains (Fig. 4 in Chapter 5).

Chapter 2

Variations in the provenance of the late Neogene Red Clay deposits in northern China

Based on: Shang Y., Beets C.J., Tang H., Prins M.A., Lahaye Y., van Elsas R., Sukselainen L. & Kaakinen A. (2016) "**Variations in the Provenance of the Late Neogene Red Clay Deposits in Northern China**". Earth and Planetary Science Letters, 439, 88-100, doi: *10.1016/j.epsl.2016.01.031*.

Abstract

The voluminous loess-Red Clay deposits in northern China forming part of the Chinese Loess Plateau (CLP) are valuable terrestrial archives of climatic evolution for the late Cenozoic Era. Fundamental in reconstructing the late Miocene and Pliocene wind patterns and aridification history is a detailed knowledge of the provenance of these deposits. This paper provides end member modelling of bulk grain-size distributions and U–Pb dating of detrital zircons for three distant Red Clay sequences in the northeastern (Baode), southern (Lantian) and western (Dongwan) CLP. Data show that these different sections each display a distinctive compositional structure indicating variable depositional processes, but they also share two significant zircon age populations of 200–300 Ma and 400–500 Ma. While the Permian–Triassic (200–300 Ma) group accounts for a larger proportion of zircons' ages in the northeastern (NE) CLP, the Ordovician–Silurian (400–500 Ma) component is dominant in the southern and western CLP. It is suggested that the Red Clay in the southern and western CLP was mainly derived from the Northern Tibetan Plateau (NTP) and the Taklimakan desert by low-level westerly winds. Samples of the NE CLP show an increased signature of sediments transported by near-surface northwesterly winds from the broad area of the Central Asian Orogen Belt (CAOB). This spatial transport and deposition pattern is supported by the results from the backtrace trajectory modelling of the dominant dust transport pathways in the CLP. It is noted that the Red Clay sample of around 3.6 Ma obtained from the NE CLP shows increased detrital contributions from its west, possibly indicating an intensified westerly wind strength and/or aridity of the NTP and Taklimakan desert due to the uplift of the Tibetan Plateau and Tianshan Mountains in the Pliocene. The onset of enhanced drainage of the Yellow River caused by the increased denudation of the NETP since 3.6

Ma could also have contributed to this.

1. Introduction

The late Neogene wind-blown sediments in the Chinese Loess Plateau (CLP) comprise two widespread units: the Miocene-Pliocene Red Clay deposits and the Quaternary loess-palaeosol sequences. These terrestrial deposits preserve valuable information for the understanding of palaeoclimatic change such as the central Asian aridification and Asian monsoon patterns during the late Cenozoic Era (An et al., 2001). The origin of the Red Clay deposits has been extensively investigated since the turn of the century and a wind-blown origin has been widely accepted (Ding et al., 1998; Sun et al., 1998b; An et al., 2001; Lu et al., 2001; Guo et al., 2002). Although generally characterized by distinct reddish fine-grained deposits with cyclic carbonate nodule-rich horizons, the sediment texture, structures and colours, degree of pedogenic alteration, and carbonate characteristics vary among different sites (Flynn et al., 2011; Kaakinen et al., 2013). A fluvial imprint in the lower part of some Red Clay successions and occasional laminated beds indicate that not all of these sections exclusively reflect an aeolian deposition (Guo et al., 2001; Zhang et al., 2013b).

The deserts and arid lands to the north and west of the CLP have long been regarded as the dust source areas of the plateau (Fig. 1) (Liu, 1985; Sun, 2002; Wu et al., 2011b). However, debate still exists over whether the aeolian Red Clay was derived from the same source region; and whether it has been transported by westerly and/or by winter monsoon winds (Ding et al., 1998; Ding et al., 2001a; Guo et al., 2004; Miao et al., 2004; Vandenberghe et al., 2004; Sun et al., 2008; Gong et al., 2015), just as it is disputed for the Quaternary loess(Sun, 2002; Chen et al., 2007; Pullen et al., 2011; Chen and Li, 2013). For example, Sun (2002) suggested that the deserts in northern China and the Gobi in southern Mongolia serve as a major dust source for the loess on the CLP whereas Chen and Li (2013) indicated that from 7 Ma to 1.2 Ma, the aeolian sediments on the CLP had been constantly supplied by the arid lands between the Qilian mountains and the Gobi Altay Mountains (GAMs).

In recent years, the use of detrital zircon U-Pb geochronology has shed new light on the provenance of Quaternary loess and constrained its source areas to the Northern Tibetan Plateau (NTP), GAMs and proximal deserts (Stevens et al., 2010; Pullen et al., 2011; Xiao et al., 2012; Xie et al., 2012; Che and Li, 2013; Stevens et al., 2013; Bird et al., 2015). Using zircon U-Pb ages, Bird et al. (2015) revealed marked spatial variability and multiple sources for the Quaternary loess: while the majority of the CLP loess originates from the northeastern Tibetan Plateau (NETP) and Yellow River (YR), the northeastern (NE) CLP receives a greater input from the northern deserts and North China Craton. Nie et al. (2015) addressed this question even further by using the extensive provenance dataset of both modern and paleo-river sediments. The findings enabled them to propose that since 3.6 Ma, substantial amounts of sediment eroded from the NETP were first carried by YR's upper reaches to the Yinchuan-Hetao Graben and from there transported by the winter monsoon winds to the Mu Us desert and eventually to the CLP. Little effort has hitherto been made to apply the single grain method to characterize the late

Neogene Red Clay strata. Zircon U-Pb dating techniques have been hampered by the small number and size of suitable grains in these fine-grained sediments. A recent study by Nie et al. (2014) provided the first zircon U-Pb provenance data of the Chaona Red Clay sequence in the central CLP. Their results revealed that the late Miocene Red Clay (8–5.5 Ma) is likely sourced both from the Qaidam basin and transported by the fluvial system from the adjacent Liupan Mountains. In contrast, the early-mid Pliocene Red Clay (5.5–4 Ma) received material mainly from the Taklimakan Desert, whereas the late Pliocene Red Clay (~ 3 Ma) had multiple origins but was dominantly sourced from the NTP.

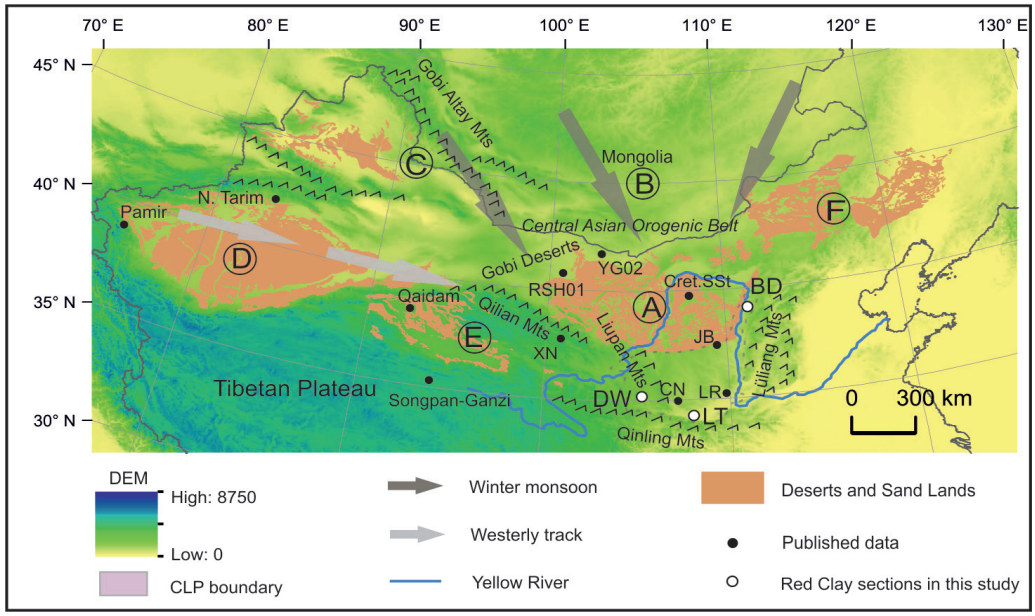

Figure 1. Digital elevation model (DEM) map of northern China. A–F represent the potential source areas for the Chinese Loess Plateau (CLP): A – deserts located north and northwest to the CLP; B – southern Mongolia Gobi desert; C – Jungger Basin (Gurbantunggut desert); D – Tarim Basin (Taklimakan desert); E – Northern Tibetan Plateau (NTP), including Qaidam Basin and Qilian Mountains; F – sandy lands in the northeastern part of the CLP. A, B, C and F are within the widespread Central Asian Orogen Belt (CAOB) in northern China on the pathway of winter monsoon winds to the CLP. D and E represent the sources in western China. The white dots mark the examined Red Clay sections within this study (BD, Baode and Jingle Fm; DW, Dongwan; LT, Lantian). The black dots indicate the locations of published zircon samples: Red Clay, CN – Chaona (Nie et al., 2014); Loess, JB – Jingbian (Bird et al., 2015), XN – Xining (Che and Li, 2013); potential source areas: YG02 (GAMs – Gobi Altay Mts source) and RSH01 (mixed source of NTP and GAMs with NTP dominating) (Che and Li, 2013), N. Tarim – northern Tarim basin samples (Li and Peng, 2010), Pamir (Bershaw et al., 2012), Qaidam and Songpan-Ganzi complex samples (Pullen et al., 2011), Cret.SSt – Cretaceous Sandstone samples (Bird et al., 2015; Stevens et al., 2013), LR – Luo River (Diwu et al., 2012).

To provide a better insight in the spatial variation of the Red Clay provenance, we selected three well known Red Clay sequences distributed across the CLP (Fig.1), namely: Baode in the northeast (Zdansky, 1923; Kurtén, 1952; Zhu et al., 2008; Kaakinen et al., 2013), Lantian in the south (Liu et al., 1960; Zhang et al., 1978; Kaakinen and Lunkka, 2003) and Dongwan in the west (Hao and Guo, 2004; Liu et al., 2011; Li et al., 2014). We employed an end member modelling approach to the grain-size distribution datasets to

characterize sediment subpopulations and their relative contributions within the three sections (cf. Prins et al., 2007) to better understand the transport and (post-) depositional processes that affect the various components. Subsequently, we applied zircon U-Pb age dating and backtrace air trajectory modelling to further explore the potential sediment sources of Red Clay as well as the prevailing wind patterns over the CLP in the late Miocene and Pliocene.

2. Material and methods

2.1. Red Clay sections

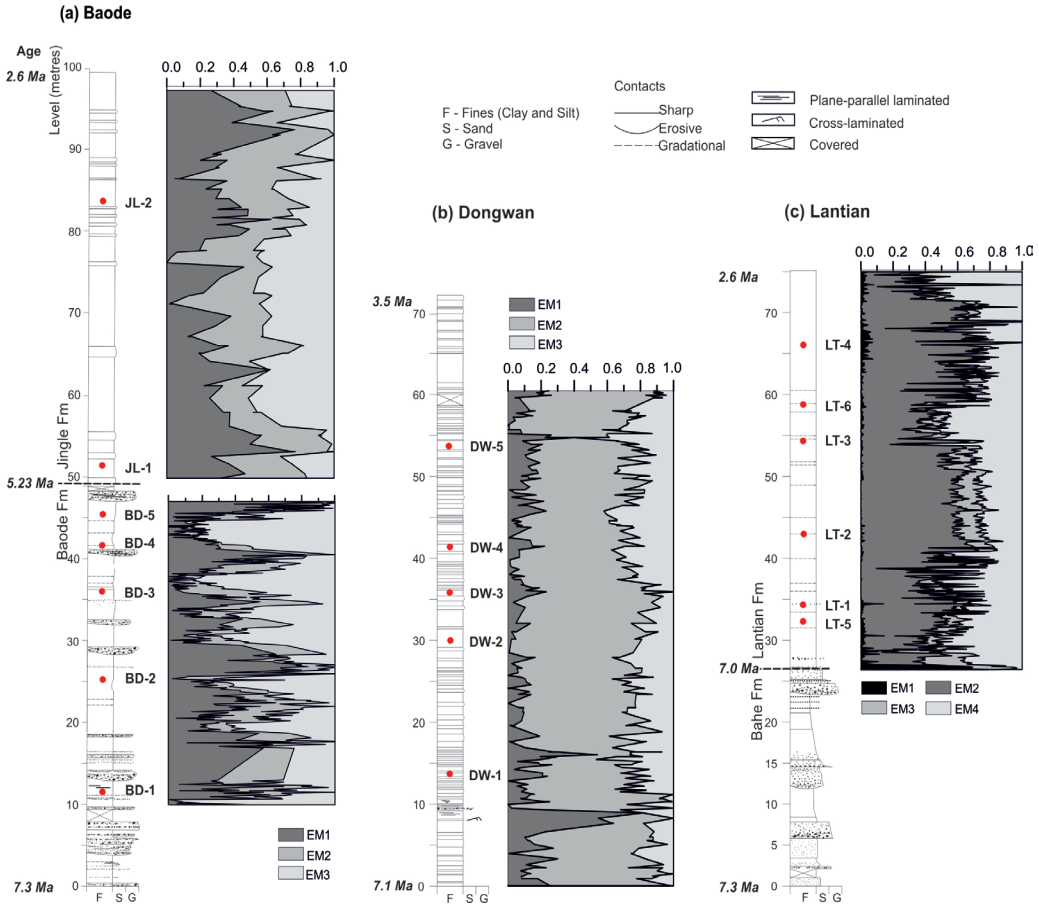

Figure 2. Lithostratigraphy of the study sites showing the proportional contributions of the modelled end members: **(a)** Baode (and Jingle), **(b)** Dongwan and **(c)** Lantian. The red dots denote locations of zircon samples in the sections. The chronology of the section is based on magnetic polarity stratigraphies by Kaakinen et al. (2013) for Baode, Hao and Guo (2004) for Dongwan and Zhang et al. (2013b) for Lantian, and sample ages were obtained by interpolating between the geomagnetic polarity boundaries.

The Liupan Mountains divide the CLP into western and eastern parts (Fig.1). Most of the Red Clay sequences on the eastern part are younger than 11 Ma (Xu et al., 2009), while those on the western part have a basal age of 22–25 Ma (Guo et al., 2002; Qiang et al., 2011). These aeolian deposits on the western CLP bear a close resemblance to the Quaternary loess and palaeosol units and therefore are also referred to as Miocene loess-palaeosol deposits (Guo et al., 2002; Hao and Guo, 2004) to differentiate them from the Red Clays on the eastern CLP. However, we follow the nomenclature of An et al. (2014) in this study and include the aeolian deposits on the western CLP along with the Red Clays.

The three Red Clay sections examined in this study represent a variety of geographical and local sedimentary settings (Fig. 1 and Fig. 2; see detailed descriptions in Supplement): 1.The Baode sequence lies in the NE CLP between the Lüliang Mountains and the Yellow River and is composed of two Red Clay formations named Baode and Jingle. 2. Lantian lies at the foothills of the Qinling Mountains and represents the southernmost occurrence of the Red Clays. 3. Dongwan is located to the west of the Liupan Mountains and represents the more loess-like Red Clays found in the western CLP. Our sampling focused on fine-grained lithologies, while for conglomerates or sandstones (Baode Fm and lowermost part of the Lantian Fm) laterally equivalent fine-grained facies was sampled.

2.2. End member modelling of grain size distributions

End member (EM) modelling of grain-size distribution (GSD) datasets (Weltje and Prins, 2007) has proven to be capable of detecting mixing patterns of sediment flux from multiple sources. The method has been designed to offer the simplest possible explanation of the observed variation among a set of compositions in terms of (un-) mixing. The EM modelling approach has been successfully used to unravel the multiple transport/deposition processes of Quaternary loess (Prins and Vriend, 2007; Prins et al., 2007; Vriend et al., 2011) but no attempt has hitherto been made to examine the underlying Red Clay.

The EM mixing models for the complete GSD datasets were produced separately for each section by the algorithm DRS-UNMIXER (Heslop et al., 2007), which is similar to the original end-member modelling algorithm EMMA (Weltje, 1997). The number of EMs was estimated in the first modelling stage based on the mean coefficient of determination (r^2) and, in the second stage, the EM compositions and their proportions in all samples were calculated. The minimum number of EMs required for a satisfactory approximation of the data was estimated by calculating the coefficient of determination (r^2), which represents the proportion of the variance of each grain size class reproduced by the approximated data (Weltje, 1997). In addition, in order to further quantify the grain-size composition of each EM, the Sand (>63 μm): Silt (8-63 μm): Clay (<8 μm; cf. Konert and Vandenberghe, 1997) (SSC) ratio of the end members were calculated.

2.3. Zircon U-Pb age dating

Descriptions of the zircon samples are given in Table 1. Zircon grains were separated

using the laboratory overflow-centrifuge (LOC-50; IJlst, 1973) with the Diiodomethane heavy liquids (density of 2.86 and 3.30 g/cm^3) and the Frantz magnetic separation techniques at the Mineral Separation Laboratory of VU University Amsterdam (VUA). The zircon U-Pb ages were then determined by using a Nu Plasma High Resolution multi-collector inductively coupled plasma-mass spectrometry (ICP-MS) at the Finnish Geosciences Research Laboratory, Geological Survey of Finland in Espoo, following a technique similar to that described in Rosa et al. (2009) except that a Photon Machine Analyte G2 laser microprobe (wavelength 193 nm) was used. Analyses were run with a laser spot diameter of 20 μm, pulse frequency of 5 Hz and beam energy density of 0.55J/cm^2. The calculations were performed off-line, using a program written in Microsoft Excel/VBA by T. Andersen (Rosa et al., 2009). Three samples (LT-5, LT-6 and JL-2) and additional zircon grains from sample BD-1, DW-3, DW-4 and DW-5 were analysed using a new single-collector high resolution ICP-MS equipment in the Geological Survey of Finland with a laser spot diameter of 21 μm (29 μm for the large zircon grains in the ranges of 60–90 μm). The raw data of the new analyses were processed by the software Glitter 4.4. $^{206}U/^{238}Pb$ and $^{207}Pb/^{206}Pb$ ages were used for ages younger and older than 1 Ga, respectively. Only ages within discordance of ±10 % were accepted in order to make it easier to compare with previously published Red Clay and loess zircon U-Pb age data for the CLP (Bird et al., 2015; Che and Li, 2013; Nie et al., 2014).

Table 1. Description of zircon samples from the three sections

section	sample ID	age(Ma)	sample size(kg)	laser spot size(μm)	No. of analysed zircon grains	No. of analysis < 10% discordance
Baode	BD-1	7.16	1.5	20	103	59
	BD-2	6.91	2	20	183	118
	BD-3	6.56	2	20	172	106
	BD-4	6.19	1.5	20	107	69
	BD-5	5.75	1.5	20	87	62
	JL-1	5.24	0.8	20	322	219
	JL-2*	3.5	0.8	21	194	83
Lantian	LT-1#	5.66	0.6	20	26	5
	LT-2	4.99	0.8	20	180	101
	LT-3#	4.38	0.7	20	17	10
	LT-4	3.7	0.8	20	54	29
	LT-5*	5.83	5	21(29)	173(164)	80(110)
	LT-6*	4.2	3.6	21	252	107
Dongwan	DW-1#	6.73	0.5	20	0	0
	DW-2#	5.81	0.6	20	61	22
	DW-3	5.47	0.6	20	106	66
	DW-4	5.26	0.6	20	236	123
	DW-5	4.46	0.6	20	80	43

Note: # samples having less than 30 analyses within 10% of discordance have been excluded from the discussion; *samples analysed with the ICP-MS single-collector; + samples analysed with both the ICP-MS multi-collector and single-collector equipment. For sample LT-5, two fractions of zircon grains were obtained after magnetic separation: 30–60 μm and 60–90 μm, analysed using a laser spot size of 21 and 29 μm, respectively.

2.4. Dust trajectory modelling

To further explore the potential transport paths of the aeolian deposits in the studied Red Clay localities, the HYbrid Single-Parcel Lagrangian Integrated Trajectory model (HYSPLIT) version 4 is employed. HYSPLIT is a well described model (Draxler and Hess, 1998), which has been applied to study dust trajectories in various regions such as Asia (Uno et al., 2009). Meteorological data including temperature, 3-dimensional wind velocity, humidity, geopotential height and surface elevation are required as inputs for the model. In this study, these data are derived from 6-hourly (10 year in total) output from a Late Miocene global model (ECHAM5/MPIOM) experiment using ~3.75×3.75° horizontal resolution and 19 vertical levels for the atmosphere (Micheels et al., 2011). This experiment has been shown to represent the Late Miocene climate reasonably well compared to other global models and thus can be used to drive the HYSPLIT model.

Three dimensional 5-days backtrace trajectories of the air mass arriving at the near surface (1000 m above ground level) of four Red Clay localities including Baode, Chaona, Dongwan and Lantian are calculated every 12 hours for both winter (December, January, February) (1784 trajectories) and spring (March, April, May) (1820 trajectories). The calculated trajectories are clustered to 4–5 mean trajectories to represent the dominant pathways of the air mass delivering dust to the sites. We choose 1000 m above ground level to initiate the backtrace trajectories, because it minimize the effect of any disturbance of the underlying topography while being sufficiently close to the terrain to be dynamically linked to the surface wind field (Sinclair et al., 2010). The uncertainties of the modelled trajectories have been shown to be 10-30% of the travel distance depending largely on the accuracy of the input data (Stohl et al., 2001). We use relatively coarse resolution global model results as the input data for HYSPLIT. This is found to be sufficient to produce present-day trajectories that compare well to those using higher resolution reanalysis data (see Supplement), and hence is considered reliable for simulating the Late Miocene trajectories.

3. Results

3.1. End member modelling

The modelled EMs and their proportional contribution in each section are shown in Fig. 3 and Fig. 2. The Baode Red Clay (the Baode Fm and Jingle Fm) was divided into three EMs (Fig. 3a and 3b). The SSC ratio of the Baode Fm EM (Fig. 3a) is 32:45:21 for unimodal BD-EM1 (modal size ~58 μm), 5:74:24 for unimodal BD-EM2 (modal size ~40 μm) and 2:46:51 for polymodal BD-EM3 (modal size ~7–21 μm). The SSC ratio for the Jingle Fm is 11:53:36 for unimodal JL-EM1 (modal size ~53 μm), 0:50:50 for unimodal JL-EM2 (modal size ~19 μm) and 9:39:52 for bimodal JL-EM3 (modal sizes ~7 and 63 μm). These ratios imply that BD-EM1 represents a sandy-silty, BD-EM2 a silty and BD-EM3 a silty-clay component for the Baode Fm. The Jingle Fm consists of more uniform sediments characterised by sandy-silty (JL-EM1) and poorly-sorted sandy to silty clay (JL-EM2 and JL-EM3) components (Fig. 3b). The SSC ratios and EM modal sizes show that the Baode Red Clay, especially the Baode Fm, is significantly

coarser than the Red Clay of Lantian and Dongwan in the southern CLP.

The Dongwan grain-size dataset was decomposed into three EMs with modal sizes at ~19 μm (DW-EM1), ~9 μm (DW-EM2) and ~6 and 26 μm (DW-EM3) (Fig. 3c). The SSC ratio is 3:65:33 for DW-EM1, 0:44:57 for DW-EM2 and 1:41:57 for DW-EM3, indicating DW-EM1 represents a silty Red Clay, whereas DW-EM2 and DW-EM3 denote clayey-silty components. The three EMs largely overlap and sand-sized particles are almost absent from all EMs, reflecting the uniform and fine-grained nature of the sediment. The high proportions of the silty DW-EM1 and the concurrent decline in the clayey DW-EM2 in the lower part of the sequence are coherent with the plane-parallel and ripple cross-laminated beds at ca. 10 and 17 m levels, indicating these deposits were water-lain.

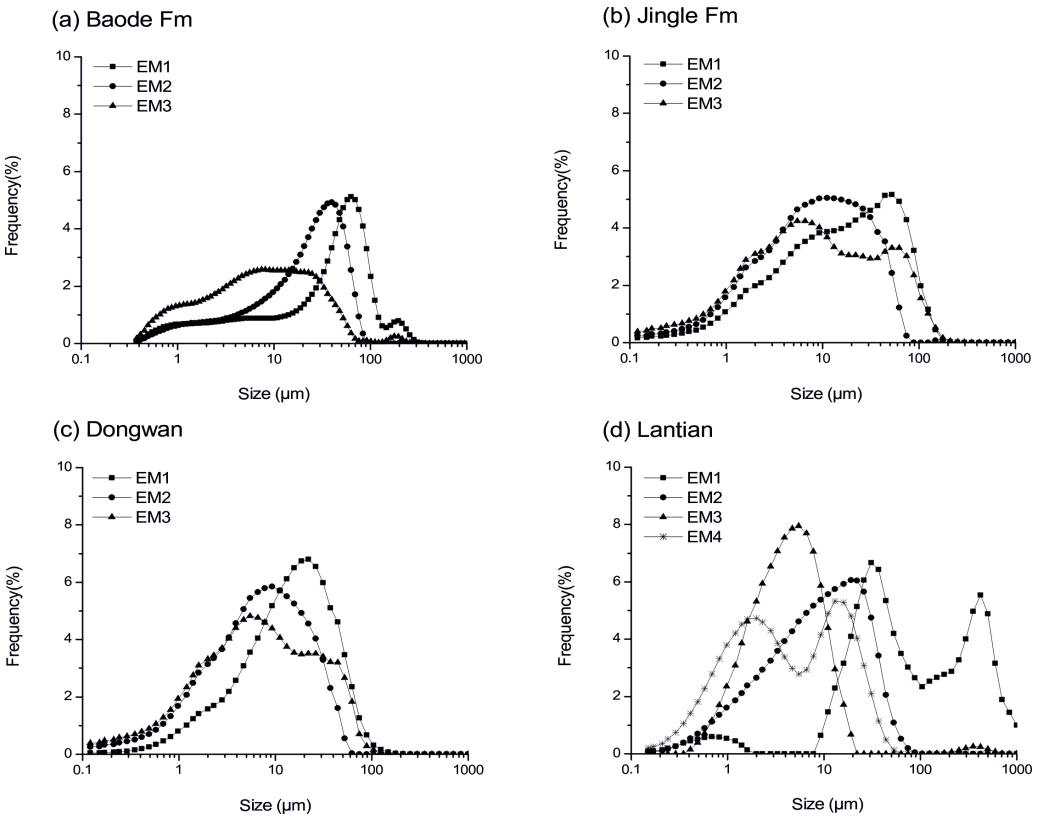

Figure 3. Grain-size distributions of the modelled end members (EMs) for the three sections. **(a)** Baode Fm: modelled end members according to a three-EM model representing sandy Red Clay (EM1, modal size ~58 μm), silty Red Clay (EM2, modal size ~ 40 μm) and clayey Red Clay (EM3, modal size ~7–21 μm). **(b)** Jingle Fm: modelled EMs according to a three-EM model representing silty Red Clay (EM1, modal size ~53 μm), and clayey Red Clay (EM2 and EM3, modal size ~19 μm and ~7 and 63 μm, respectively). **(c)** Dongwan: modelled EMs according to a three-EM model representing silty Red Clay (EM1, modal size ~19 μm), clayey Red Clay (EM2 and EM3, modal size ~9 μm, ~6 and 26 μm, respectively). **(d)** Lantian Fm: modelled EMs according to a four-EM model representing sandy Red Clay (EM1, modal size ~31 and 420 μm), silty Red Clay (EM2, modal size ~40 μm) and clayey Red Clay (EM3 and EM4, modal size ~6 μm, ~2 and 13 μm respectively).

The EM modelling of Lantian shows a more complex structure in being decomposed into four EMs, including two bimodal EMs (Fig. 3d). The SSC ratio is 50:49:5 for LT-EM1 (modal size ~31 and 420 μm), 0:52:49 for LT-EM2 (modal size ~40 μm), 1:16:81 for LT-EM3 (modal size ~6 μm) and 0:35:65 for LT-EM4 (modal size ~2 and 13 μm), which suggests LT-EM1 represents a sandy, LT-EM2 a silty, LT-EM3 and LT-EM4 a clayey component. Both LT-EM3 and LT-EM4 are dominated by clay size grains, but the clay proportion is significantly higher in LT-EM3 (81%) than in LT-EM4 (65%). In addition, with a modal size at 6 μm, LT-EM3 is comprised of a more purely clayey fraction while LT-EM4 is bimodal with peaks at 2 and 13 μm. The stratigraphic distribution of the EM proportions reveals synchronous changes in LT-EM2 and LT-EM3, whereas LT-EM4 performs in an opposite way suggesting LT-EM3 underwent the same transport/deposition process as LT-EM2. Fig. 2 also displays that the silty (LT-EM2) and clayey (LT-EM4) components dominate the major part of the Lantian Fm and the sharp increase of the sandy (LT-EM1) and silty (LT-EM2) EMs at ca. 25–30 m reflect the fluvial influence in the formation boundary.

3.2. Detrital U-Pb ages

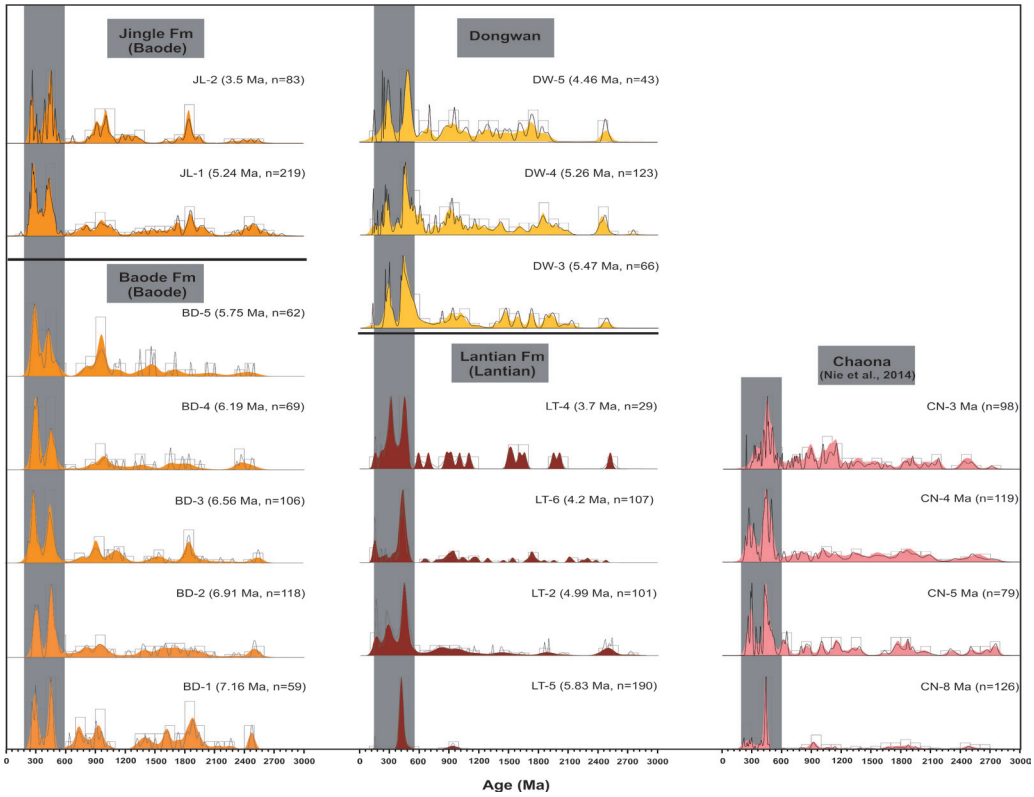

Figure 4. Detrital zircon U–Pb ages for the Red Clay samples analysed within this study and the previously published Chaona Red Clay dataset (Nie et al., 2014). Black lines are normalised probability density function plots (PDP); the orange, yellow, red and pink colours refer to Kernel Density Estimation (KDE) plots for Baode, Dongwan, Lantian and Chaona, respectively; the open rectangles are age histograms and the grey bars highlight the major age populations in the plots.

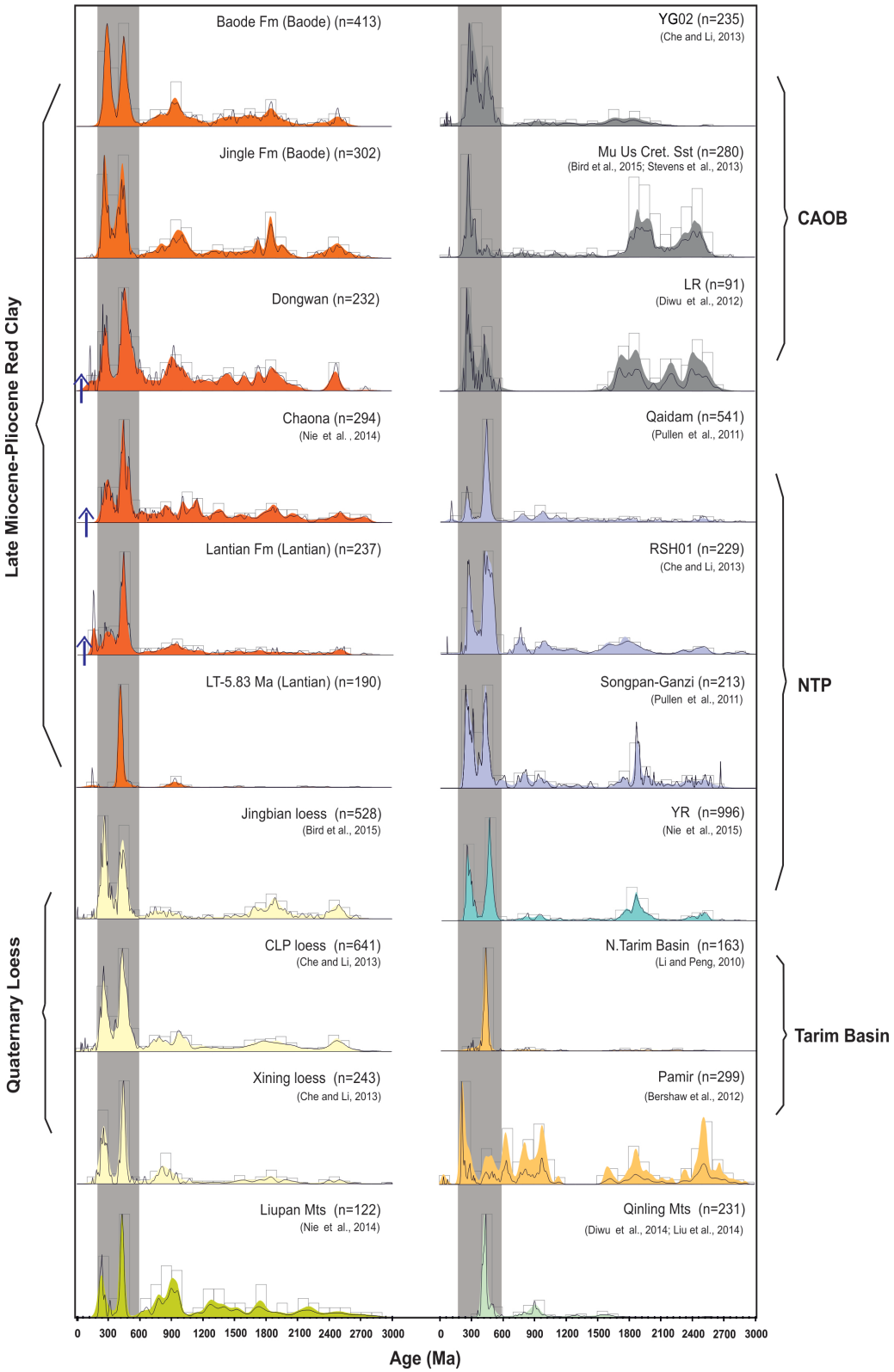
Baode Fm (Baode) (n=413)
Jingle Fm (Baode) (n=302)
Dongwan (n=232)
Chaona (n=294)
(Nie et al., 2014)
Lantian Fm (Lantian) (n=237)
LT-5.83 Ma (Lantian) (n=190)
Jingbian loess (n=528)
(Bird et al., 2015)
CLP loess (n=641)
(Che and Li, 2013)
Xining loess (n=243)
(Che and Li, 2013)
Liupan Mts (n=122)
(Nie et al., 2014)
YG02 (n=235)
(Che and Li, 2013)
Mu Us Cret. Sst (n=280)
(Bird et al., 2015; Stevens et al., 2013)
LR (n=91)
(Diwu et al., 2012)
Qaidam (n=541)
(Pullen et al., 2011)
RSH01 (n=229)
(Che and Li, 2013)
Songpan-Ganzi (n=213)
(Pullen et al., 2011)
YR (n=996)
(Nie et al., 2015)
N.Tarim Basin (n=163)
(Li and Peng, 2010)
Pamir (n=299)
(Bershaw et al., 2012)
Qinling Mts (n=231)
(Diwu et al., 2014; Liu et al., 2014)
Late Miocene-Pliocene Red Clay
Quaternary Loess
CAOB
NTP
Tarim Basin
0 300 600 900 1200 1500 1800 2100 2400 2700 3000
Age (Ma)

Figure 5 (in page 42). Combined zircon U–Pb ages from Red Clay samples in this study and previously published data. The black lines are normalised probability density function plots (PDP); the colour filled areas are Kernel Density Estimation (KDE) plots for different units; the open rectangles are age histograms and the gray bars highlight the major agepopulations in the plots. The blue arrows indicate upsection increases of the 200–300 Ma age components. For data sources see the description in Fig. 1. Tarim Basin and NTP sources are represented by areas of D and E respectively, CAOB sources – GAMs and Cret.SSt correspond to the area of C and A, respectively in Fig. 1. The combined Red Clay data exclude Lantian and Chaona samples LT-5 (5.83 Ma) and CN-8 Ma because their zircon age distributions are distinct from the rest of the samples in the same sections (Fig. 4).

Fig. 4 displays the zircon U-Pb age distributions for samples from Baode, Lantian and Dongwan and for a previously published Chaona Red Clay section (Nie et al., 2014). The results show that the ages of all samples spread from early Jurassic to Precambrian, with two dominant Permian-Triassic and Ordovician-Silurian age populations at 200–300 Ma and 400–500 Ma. The exception to this is LT-5 (5.83 Ma) for which the 200–300 Ma age population is found to be nearly absent. The 400–500 Ma peak is most prominent in all Lantian and Dongwan samples apart from LT-4 (3.7 Ma) and DW-5 (4.46 Ma) in which the zircon grains might be too few to establish a meaningful comparison. For the Jingle and Baode samples, the magnitude of the two major age populations is almost equal in BD-1 (7.16 Ma), BD-2 (6.91 Ma) and JL-2 (3.5 Ma), whereas the 200–300 Ma age population dominates the other samples. It is noticed that the proportion of 400–500 Ma age population increased from 17% for sample JL-1 (5.24 Ma) to 20.5% for JL-2 (3.5 Ma) in the Pliocene (Fig.4). For each section, the number of zircon grains older than 600 Ma defines minor peaks at the ranges of 0.8–1 Ga, 1.5–2.0 Ga and ca. 2.5 Ga.

According to Pullen et al. (2014), large numbers (n = 300–1000) in the zircon age dataset will substantially increase the statistical robustness of the analysis and allows for quantitative comparisons between samples with multiple age components. Therefore, as an attempt to this approach, we combined zircon ages from individual formations at the sites in Fig. 5 to generate large-n dataset and to assess differences between the data of our study and previously published late Miocene-Pliocene Red Clay sites (Nie et al., 2014), Quaternary loess (Bird et al., 2015; Che and Li, 2013) and the potential source areas (Li and Peng, 2010; Pullen et al., 2011; Bershaw et al., 2012; Diwu et al., 2012; Che and Li, 2013; Stevens et al., 2013; Diwu et al., 2014; Liu et al., 2014a; Bird et al., 2015). The combined Red Clay dataset not only repeats the pattern seen in the individual samples (Fig. 4), but the data also exhibit a southward decrease in the proportion of the 200–300 Ma zircon age population from Baode to Dongwan to Chaona and to Lantian.

Non-matrix Multi-Dimensional Scaling (MDS) maps (Vermeesch, 2013) used to visualise the (dis) similarities between the large zircon datasets of Red Clay, loess and the potential source areas. Detailed description of this method is in the supplement. The 2D non-metric MDS map of the combined Red Clay and loess data (Fig. 6a) reveals that the Jingle and Baode samples are almost identical and they lie close to the Quaternary loess (CLP loess) from Caoxian and Xifeng and also show similarity to Jingbian loess in the NE CLP. Dongwan samples overlap with those from Chaona as do the Lantian Red Clay samples with Xining Loess. The lowermost Lantian Fm sample (LT-5; 5.83 Ma) plots separately from other samples from the same section.

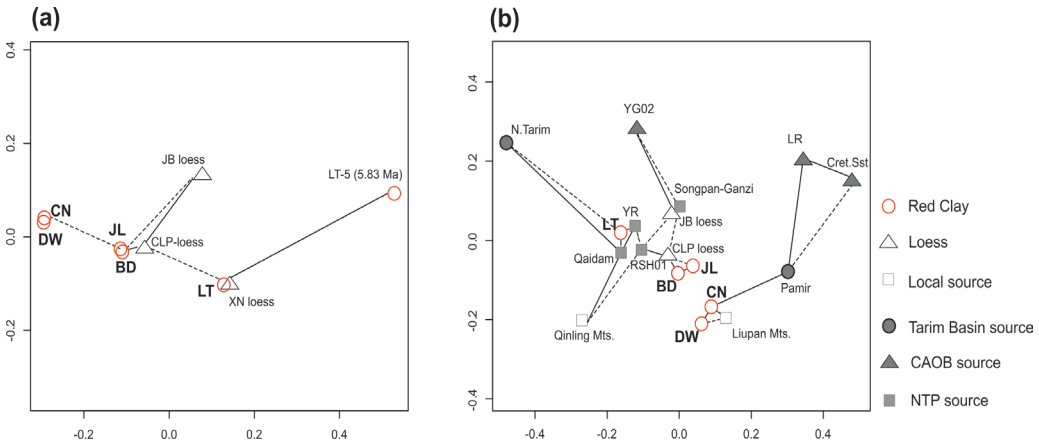

Figure 6. Non-metric multi-dimensional scaling (MDS) map: **(a)** combined Red Clay and Quaternary loess dataset; **(b)** combined Red Clay and Quaternary loess dataset and the potential source areas. The stress value is 0.0075% and 7.35% for (a) and (b), respectively, indicating a good fit of the data. The solid lines link the closest neighbours and the dashed lines the second closest neighbours. The data used here are same as described in Fig. 1 and Fig. 5. Note that the relationships shown in the map are one-way indications rather than mutual connections. For example, Jingbian loess is the most similar sample to the GAMs sample (YG02), whereas Jingbian loess shows closest affinity with the Songpan–Ganzi sample.

The zircon U-Pb age MDS plot for the combined Red Clay, loess and the potential source regions (Fig. 6b) reveals that Lantian Red Clay plots close to the zircon samples from Qaidam (Pullen et al., 2011), Ruoshui River (RSH01; Che and Li, 2013), and YR (Nie et al., 2015), which mainly represent the material from the NTP. Baode and Jingle samples display similarity with Ruoshui River fluvial sediments, which represent mixed sources from NTP and GAMs (Che and Li, 2013), whilst Dongwan and Chaona plot close to the Liupan Mountains. Neither of the N.Tarim basin (Li and Peng, 2010), Pamir (Bershaw et al., 2012) and GAMs samples (YG02; Che and Li, 2013) cluster with the Red Clay samples in the MDS map. However, this cannot be simply interpreted as these regions being of little importance in providing dust for Red Clay, since the Red Clay deposit may represent a mixture of these distant dust sources with distinctly different zircon ages and thus exhibiting little resemblance to any of the individual source regions.

3.3. Dust trajectory modelling

Fig. 7 illustrates the modelled late Miocene pattern of the 5-day backtrace air trajectories in winter for the four Red Clay sites. The trajectories in spring are similar to those in winter and are thus not shown. Our results suggest that the overall long-distance trajectories of air mass transporting dust to Baode may have been more northerly in direction than those to Lantian, Dongwan and Chaona in the late Miocene. We also calculated the ratios of the trajectories passing through the major dust source regions for each locality in winter (Fig. 7e). All the four sites were found to be dominantly influenced by the trajectories crossing the northern deserts and Inner Mongolia (A), southern Mongolia (B) and the Jungar Basin (C), where the zircon ages range between 200–600 Ma (Briggs et al., 2007; Xie et al., 2007; Xie et al., 2012). However, there is a clear increasing trend

from Baode to Lantian to Chaona/Dongwan in the proportion of trajectories crossing the western deserts in the Tarim Basin (D) and the NTP (E), with the 400–500 Ma zircon age populations predominating (Li and Peng, 2010; Pullen et al., 2011; Xie et al., 2007), whereas the proportion of trajectories crossing the north-eastern deserts, such as Horqin and Otindag sandy lands (F) decreases (Fig. 7e).

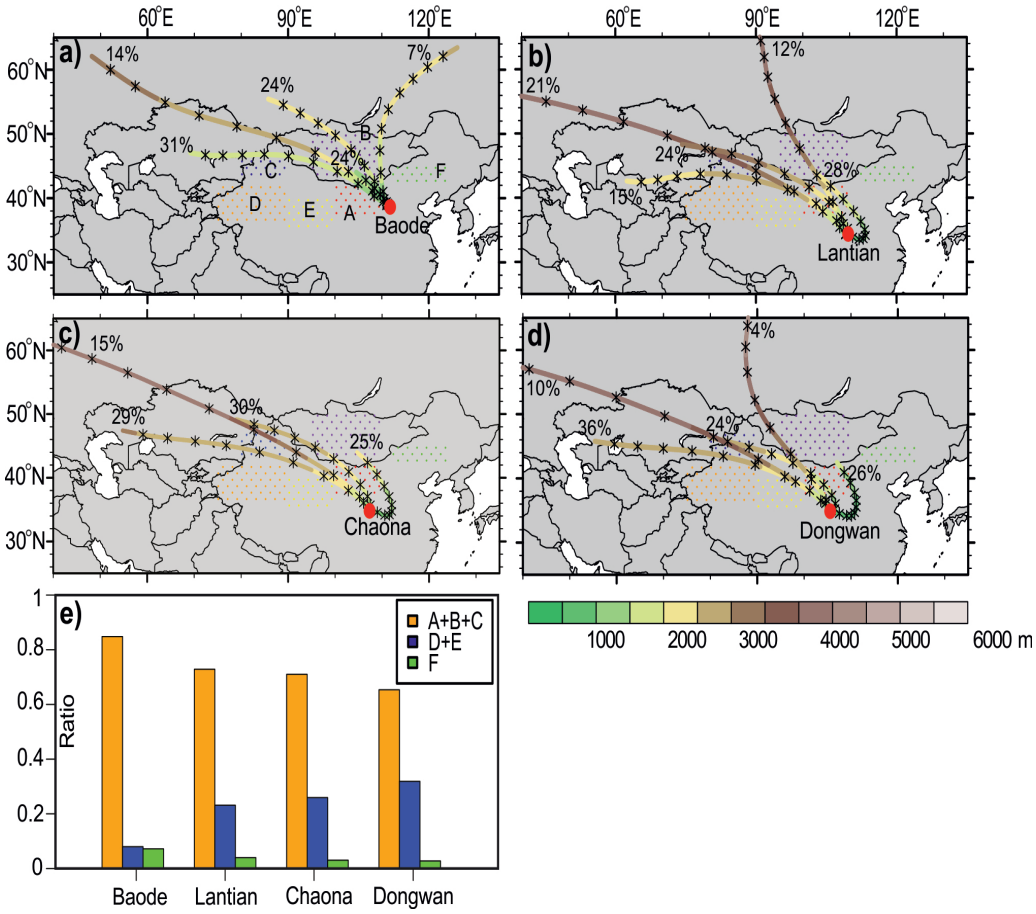

Figure 7. The cluster-mean 5-days backtrace trajectories in winter for the studied localities using HYSPLIT model: **(a)** Baode, **(b)** Lantian, **(c)** Chaona and **(d)** Dongwan. The colours of the trajectories denote their heights and the asterisks denote the locations of air parcels at 12 hourly intervals. The number along each cluster-mean trajectory denotes the percentage of trajectories belonging to the cluster. The coloured dotted areas denote the potential dust sources similar to that in Fig. 1. The ratios of the number of trajectories passing over the northern deserts (A, B, C), the western deserts (D, E) and the eastern deserts (F) for different localities are shown in **(e)**.

4. Discussion

4.1. Spatial heterogeneity of the modelled Red Clay components

The EM grain-size distribution of Red Clay is found to vary between the localities and its components are complex mixtures with clear bimodal GSD patterns. This is different from the typical EMs of Quaternary loess that are characterised by a unimodal, fine-skewed grain-size distribution with modal size at ~63 μm (EM1), ~37 μm (EM2), and ~22 μm (EM3) (Prins and Vriend, 2007; Prins et al., 2007; Vriend et al., 2011). Hence additional care should be taken in explaining the transport and (post-) depositional processes for the EMs of Red Clay depending on its local stratigraphic and sedimentological characteristics. Overall, the distribution of EMs reflects not only the difference between silty Red Clay in the NE CLP to clay-rich Red Clay in the southern CLP, but also characterises the different stratigraphic units in terms of their contributions (Fig. 2).

The stratigraphic variation is most evident in the Baode Fm (Fig. 2a), where the sandy and silty EMs (BD-EM1 and BD-EM2) peak in phase with the cyclically occurring fluvial coarse-grained units. These fluvial beds with sharp lower and upper contacts are nevertheless considered to represent short-lived, local fluvial action in the area. We suggest, therefore that the coarse-grained component BD-EM1 and BD-EM2 are partly fluvial sediments. In contrast, the transport mode for the fine-grained deposits (BD-EM3) in the Baode Fm is interpreted as primarily aeolian, although GSDs and a few sedimentary structures reveal that many of these beds have partly undergone transport by surface runoff or fluvial reworking after initial aeolian deposition. The field observations and GSDs clearly demonstrate the aeolian origin of the Jingle Fm and the distribution pattern of the three EMs of the Jingle Fm is also comparable to that of Quaternary loess (Prins and Vriend, 2007; Prins et al., 2007; Vriend et al., 2011), except the clayey fraction (JL-EM3), which shows bimodality. The fine-grained sand fraction (11% in JL-EM1 and 9% in JL-EM3) may have also been transported by aeolian suspension processes (cf. Prins et al. 2007) and can be attributable to the proximity of the source and/or stronger NW winter monsoon winds. A fluvial influence can be excluded based, for example, on the ubiquitous silty texture of the formation, lack of hydraulic structures and spatially correlative lithostratigraphy over vast areas. For the Red Clay in Dongwan and Lantian in the southern CLP (Figs 2b and 2c), the sandy (LT-EM1) and silty (DW-EM1) EMs in the lower part of the section represents the influence of fluvial or water-laid sediment while the silty and clayey component (LT-EM2, LT-EM3 and DW-EM2) are mainly fine-grained aeolian deposits.

Notably, the GSDs of the clayey sub-fraction in the Jingle Fm (JL-EM3), Dongwan (DW-EM3) and Lantian (LT-EM4) are all characterised by two distinct modal sizes (Fig. 3), a feature not observed for the Quaternary loess-palaeosol sequences. The EM modelling results show this particular group of clayey EMs represents a fraction in the Red Clay that cannot be further unmixed. Vandenberghe et al. (2004) found that there is no obvious correlation between magnetic susceptibility and grain size in the upper

portion of Xifeng Red Clay in the northern CLP; hence they concluded that the clay fraction of the main part of Xifeng Red Clay may not have had a pedogenic origin but was transported by wind. In contrast, Sun et al. (2006b) indicated that the GSD of the original Red Clay deposits may have been modified by the post-depositional pedogenic processes. More intensive weathering and pedogenic processes are generally seen in the southern CLP than the northern CLP for both the Quaternary loess and the underlying Red Clay. We suggest, therefore, that those bimodal clayey EMs, i.e. JL-EM3, DW-EM3 and LT-EM4 represent an aeolian dust component that has been subjected to post-depositional pedogenic processes, thus exhibiting a mix of silty quartz grains and in-situ produced clay minerals. Although more detailed analysis has to be done to quantify the aeolian proportion in the clay fraction, we propose that the proportion of this biomodal EM in the bulk Red Clay could be a potential index for the weathering degree. For example, the average proportion of the bimodal clayey EM in the Lantian Fm (LT-EM4) is 35.0% while that in the Dongwan section (DW-EM3) is 22.2%, indicting a more intensive pedogenic process in the Lantian area. This is well in agreement with the field observations implying that the Miocene-Pliocene aeolian sediment sequences to the west of the Liupan Moutains are more loess-like and less weathered than the Red Clay deposits to the east of it (Guo et al., 2002; Qiang et al., 2011). In addition, the southern CLP sites of Dongwan and Lantian have relatively uniform zircon U-Pb age distributions but deviate in EM compositions suggesting a similar provenance but differing post-depositional processes due to local climatic conditions.

4.2. Spatial variation in the provenance of Red Clay

With a dominant age peak at 400–500 Ma, Lantian Red Clay (except LT-5) yields a similar zircon age distribution as Xining loess, Ruoshui River, Qaidam Basin and terraces in the upper reaches of the YR (Fig. 5 and Fig. 6), that have their origins in the NTP. This suggests that sediments eroded from the NTP dominate the sources of the Lantian Red Clay. It is feasible that zircons with an age of 400–500 Ma could also have come from the Taklimakan deserts in the far west, as suspected upon the similar zircon age spectra (Li and Peng, 2010; Xie et al., 2007). Sample LT-5 (5.83 Ma) of the Lantian section stands out because of its dominant 400–500 Ma age population and an absence of the 200–300 Ma age group. A comparison between LT-5 and the rest of the Lantian samples shows that the former yields a larger proportion of euhedral prismatic zircon grains whereas the amount of rounded zircon grains in the overlying samples is higher. In addition, the age mode of LT-5 is around 420 Ma while that of the other Lantian samples is 450 Ma. The lower part of the Lantian Fm is often associated with conglomerate beds. The fact that the bulk GSD of LT-5 shows an apparent sandy proportion (Supplement, Fig. S1), indicates that this sample (level) has most likely been influenced by flowing water and these euhedral zircon grains were likely locally derived from the Silurian-Devonian magmatic rocks in the Qinling Mountains (Meng and Zhang, 2000; Ratschbacher et al., 2003; Diwu et al., 2012; Diwu et al., 2014; Liu et al., 2014a). In contrast, a fluvial origin can be excluded for the overlying Lantian samples, as there are no signs of hydraulic structures found in these samples (Fig. 2) and the bulk GSD also shows a typical aeolian Red Clay pattern (Fig. S1 in Supplement).

The Dongwan U-Pb age distributions compare well with those of Lantian and are nearly identical with Chaona early Pliocene (5.5–4 Ma) samples in the central CLP (Fig. 4-6), suggesting a similar source for both sites. However, information derived from the U-Pb age spectra in this case is inconclusive because both the Taklimakan desert and NTP have a predominant 400–500 Ma age component (Li and Peng 2010; Pullen et al., 2011; Xie et al., 2007). We notice that Dongwan contains smaller zircon grains than Lantian (Supplement, Fig. S2), a finding that favours a longer transport distance for the particles. Therefore, it is possible that a larger proportion of the Dongwan zircons were transported from the more distant Taklimakan area. However, in the MDS map, Dongwan samples do not plot close to any of these samples from the Taklimakan margin area, such as N. Tarim and Pamir (western Tarim) (Fig.6). This is likely because the Taklimakan desert received sediments from its surrounding mountains, and therefore the age distribution found in the central Taklimakan desert (Fig.3 in Xie et al., 2007 and Fig.2 in Nie et al., 2014) is actually a mix of western and northern Tarim sources. The MDS plot shows that the Dongwan and Chaona Red Clay samples plot closer to the Liupan Mountains rather than to other source areas. Although local windblown input from the Liupan Mountains is possible, the ubiquitously small grain sizes and a near lack of fluvial sedimentary structures in the Dongwan sequence argue against significant fluvial contributions from a proximal source.

The U-Pb age spectra of the Baode and Jingle Red Clay exhibits a high level of similarity with the Quaternary loess, which is closely affiliated with the NTP sources (Bird et al., 2015; Nie et al., 2015; Pullen et al., 2011; Stevens et al., 2013) (Fig. 5 and Fig. 6). The prevailing 200–300 Ma zircon age population in the Baode and Jingle Red Clay resemble the dominant signature in the sediments that were eroded from the Central Asian Orogen Belt (CAOB) – the GAMs and the Cretaceous sandstones underlying the eastern Mu Us desert (Bird et al., 20142015; Che and Li, 2013; Stevens et al., 2013) – suggesting that these were important sources areas for the NE CLP Red Clay. Compared to the southern site, Baode and Jingle Red Clay are more silt-dominated (Figs. 2 and 3) with coarser zircons grains (Supplement, Fig. S2), indicating that the neighbouring eastern Mu Us was a more favourable candidate source than the remote GAMs and southern Mongolia. Although the MDS map shows that none of the CAOB samples lies close to the Baode and Jingle samples, this can be justified, considering the zircons age spectra in Baode and Jingle represent a mixture of detritus sourced from both the NTP and the CAOB rather than from one single area.

Overall, our zircon data seem to reveal that whereas the NTP source dominates the Lantian Red Clay in the southern CLP, it contributes a component to the NE CLP Baode deposits. Thus, our results are consistent with the findings of previous studies on Quaternary loess and Pliocene Red Clay, which indicate that the eroded material from the Qilian Mountains and Qaidam desert of the NTP was an important dust source for the CLP (Bird et al., 2015; Che and Li, 2013; Chen et al., 2007; Chen and Li, 2013; Nie et al., 2014; Pullen et al., 2011). The 200–300 Ma zircon age population gradually increases in proportion from Lantian to Dongwan/Chaona and to Baode, suggesting more input from the CAOB sources to the NE CLP region. Similarly, the Quaternary Jingbian loess located in the NE CLP also exhibits a dominant signature of the CAOB (i.e. eastern Mu

Us desert) source, whereas the majority of the CLP Quaternary loess shows a strong NTP source signal (Bird et al., 2015). This together with our results implies that a consistent spatial variation in the provenance of wind-blown sediment of the CLP having occurred since at least the late Miocene.

Our backtrace trajectory model results coincide with the above spatial pattern, revealing a larger proportion of wind trajectories passing over the CAOB source region (e.g., the Mu Us desert and GAMs) to Baode, than to the southern localities of Lantian, Chaona and Dongwan (Fig. 7). This indicates that the large-scale winter monsoon wind pattern, i.e., the relative strength of the westerly and northerly wind, may have contributed to the spatial variation in the zircon provenance of the CLP Red Clay. However, we notice some inconsistences between the modelled trajectories and zircon provenance data. For instance, our zircon data indicate that dust from the west, i.e. the NTP, are generally dominant in the CLP Red Clay, while the modelled trajectories show more wind trajectories coming from the north than from the west (Fig. 7e). Such discrepancies can be due to the model biases caused by its global climate forcing data (see Supplement 4). In addition, trajectory model only tells the potential air routes for bringing dust. It considers neither the availability of dust in the source regions nor the dust loading capacity of the trajectories, and thus may be incomplete in reflecting the strength of dust transport along each trajectory.

It is noted that most zircons analysed in this study are in the silt fraction (20–60 μm), which could limit the source areas towards the more proximal areas (e.g., eastern Mu Us desert and the NTP) and thus may underestimate the contribution of the distal sources. In particular, the Taklimakan desert as a possible distant source for the southern CLP (Dongwan and Lantian) is noteworthy. Sun et al. (2009) dated the oldest aeolian dune sands in the central Taklimakan desert at ca. 7 Ma while recent evidence from volcanic ash layers suggests an earlier formation of Taklimakan at the late Oligocene to early Miocene (Zheng et al., 2015). This indicates that the Taklimakan desert could have served as a significant dust source area for the CLP since at least the late Miocene. In addition, according to Bian et al. (2011), relatively coarse dust particles may also be transported from a remote dust source region, such as the Taklimakan desert, to the CLP through a step-wise transport (i.e., the so-called “propagate dust source process”). Our modelling results show that most of the dust trajectories to the CLP are confined to the lower troposphere (less than 3000 m above the ground) that is dynamically linked to the surface (Fig. 7). This would allow wind to pick up dust from the surface below easily, therefore favouring a step-wise dust transport. To better understand the dust entrainment process and the spatial variation in the provenance of Red Clay, experiments using a fully-fledged dust model coupled with atmospheric model would be needed.

4.3. Climate implications from the Red Clay deposits since the late Miocene

The spatial distribution of Red Clay provenance and dust trajectories modelling reveal that at least two wind components during winter and spring probably influenced the dust transportation to the CLP area in the late Miocene: the northerly and north-westerly

wind in the lower troposphere that was more dominant in the northeastern CLP, and the westerly wind more prevalent in the southern CLP. It should be noted that the term "westerly wind" we use here has the same meaning as mentioned by Nie et al. (2014), referring to the wind directly from the west to the CLP including not only the high level jet stream but also the low-level westerly wind. The latter is an important component of the Asian winter monsoon system (Chang et al., 2006). A recent study by Tang et al. (2015) has suggested that the late Miocene winter monsoon is characterized by a large westerly component compared to the present. This is consistent with our observation that NTP detrital material serves as an important source for the late Miocene–Pliocene Red Clay.

A possible change of provenance in the NE CLP Red Clay that occurred in the middle Pliocene (around 3.6 Ma) is suggested by the increase of the 400–500 Ma zircon age population in the upper Jingle Fm (JL-2, Fig. 4). Even though this is based on a smaller number of zircon grains (n=83), it may indicate that the Jingle Red Clay in Baode might have been receiving an increased contribution of dust from western China since the middle Pliocene. For the Lantian and Dongwan localities, we have too few grains in their Pliocene samples to determine reliable zircon age spectra and thus cannot ascertain a temporal trend from the late Miocene to Pliocene. However, supporting evidence for an increased dust supply from western areas in the mid-Pliocene comes from the Chaona sequence in the middle CLP where source materials from the sediments in the middle-northern Tibetan Plateau are found to dominate its ~3 Ma late Pliocene sample (Nie et al., 2014). This also points to an increased dust input into the CLP from the west in the middle–late Pliocene. We attribute this change to either a stronger (weaker) westerly (northerly) wind component, or/and intensified aridity of the dust source regions in the NTP and the Taklimakan desert areas in the Pliocene. Intensified aridity of the NTP and Taklimakan in the Pliocene as documented by pollen records in the Qaidam Basin (Wu et al., 2011a) and multiple geochemical proxies from the Tarim Basin (Liu et al., 2014b; Liu et al., 2015) has been ascribed to the uplift of the NTP and Tianshan Mountains during the Pliocene. As a consequence, westerly winds to the CLP were enhanced according to a recent climate model simulation (Fig.10d in Zhang et al., 2015). The combination of these lines of evidence implies that the growth of the NTP played an important role in the increase of dust input from the western source regions to the CLP in the Pliocene. Moreover, recently Nie et al. (2015) proposed that YR sediments derived from the erosion of the NETP are largely stored as loess in the CLP after 3.6 Ma due to the increased NETP denudation and enhanced fluvial activity. The onset of enhanced YR drainage at 3.6 Ma, thus, may provide an additional explanation for the change of Red Clay provenance to more western sources in the middle Pliocene. More provenance studies based on high-resolution samples and large dataset are still needed to fully answer this question.

5. Conclusions

EM modelling and zircon U-Pb dating, combined with the dust trajectory modelling for the three Red Clay sections on the CLP reveal the provenance variations of the Red Clay since the late Miocene. Our results favour a combination of northerly and westerly

sources from the late Miocene to the middle Pliocene. The more clay-dominated Red Clay in the southern (Lantian) and western (Dongwan) CLP sites mainly received material from the NTP and the Taklimakan desert transported primarily by low-level westerly winds. The more silt-dominated Red Clay of Baode and Jingle Fm in the NE CLP shows a larger proportion of dust transported by northwesterly and northerly winds from the broad area of the CAOB. An increased dust component from western China appears from 3.6 Ma, indicating an intensified westerly-driven winter monsoon and/or aridity of the NTP and Taklimakan desert attributed to the uplift of the NTP and Tianshan Mountains, and perhaps to the onset of enhanced YR drainage due to increased NTP denudation.

Supplementary material

S.1. Site description and stratigraphy

Baode in the northeastern CLP lies west of the Lüliang Mountains and east of the Yellow River (Fig. 1). Neogene sediments underlying the Quaternary loess-palaeosol deposits are grouped into two Red Clay formations (Fig. 2), the late Miocene Baode Fm and Pliocene Jingle Fm. The Jingle Fm is composed exclusively of fine-grained deposits and exhibits deeper red colour while the underlying Baode Fm shows a more variable lithology and overall upward-fining succession with conglomerate interbeds. Rich mammalian fossil assemblages have been recorded from several levels in the Baode Fm, whereas the Jingle Fm is almost devoid of them (Kaakinen et al., 2013). Magnetic polarity stratigraphy (Kaakinen et al., 2013; Zhu et al., 2008) demonstrates that the Baode Fm started to accumulate 7.23 Ma ago and the composite Jingle Fm represents the time interval from 5.34 to 2.72 Ma. The southernmost site Lantian lies in the Weihe Graben adjacent to the Qinling Mountains and comprises a thick accumulation of Cenozoic clastic sediments. The late Neogene sedimentary infill of the graben consists of the Bahe and its overlying Lantian Fm totalling more than 300 m in thickness (Kaakinen and Lunkka, 2003; Zhang et al., 2013b). Based on geochemical and grain size evidence, the fine-grained units of the Bahe Fm have been suggested to be partly aeolian (Wang et al., 2014). The overlying Red Clay succession (Lantian Fm) is characterized by distinct deep-red fine-grained deposits in which the cyclic carbonate nodule rich horizons become progressively more abundant in the upper part of the formation. Fossil mammal localities coincide with minor fluvial components of the lowermost 5–10 metres of the formation. Paleomagnetic studies (Wang et al., 2014; Zhang et al., 2013b) date the basal age for the Bahe Fm to 11 Ma and place the boundary between the Bahe and Lantian Fm at 7 Ma. Dongwan is located in the western CLP and its Red Clay sequence is composed of a 74-m-thick succession of reddish silt and carbonate rich couplets with fossil micromammals (Liu et al., 2011) and terrestrial molluscs (Li et al., 2014) throughout the sequence. The silt beds are dominantly massive, although thin lamination indicating water-lain settling is recognized at ca. 8–10 m and 17 m levels (Fig. 2). Unlike the Jingle Fm in Baode and the Lantian Fm, the carbonate units in Dongwan show only weak nodule formation. The timescale for Dongwan (7.1 to 3.52 Ma) is based on the magnetostratigraphy of Hao and Guo (2004).

S.2. Bulk grain size analysis

For grain size analysis, approximately 0.5–1 g of bulk sediments was pre-treated with H2O2 and HCl to remove carbonate and organic matters following a standard procedure for Red Clay (cf. Konert and Vandenberghe, 1997; Vandenberghe et al., 2004). Samples (n=282) from Baode Fm were analysed with a Coulter LS200, samples (n=493) from Lantian Fm with a Fritsch A22, and samples from Jingle Fm (Baode) (n=54) and Dongwan (n=133) with a Sympatecs KR laser diffraction particle sizer. These laser-diffraction instruments provide grain size measurements in the range of 0.15–2000 μm.

S.3. Statistical approach for zircon U-Pb ages

The zircon U-Pb age distributions of each Red Clay sample were displayed by Probability Density Plots (PDP; Ludwig, 2003), Kernel Density Estimation (KDE; Vermeesch, 2012) plots and histogram diagrams to make visual comparison. We aimed to obtain more than 100 zircon grains for each sample within the limit of ±10 % discordance since this is considered as a relatively reliable dataset to characterize the sediment composed of detritus from multiple source areas (Vermeesch, 2004; Andersen, 2005). However, because a large proportion of zircon grains are too small or fractured for analyses, only seven samples achieved the target (Table1). In order to reduce the bias and statistical error induced by the smaller sample sizes, we grouped the zircon ages together for all samples from the individual formations at the sites to display a more representative sample of zircon ages with enough analyses for each unit. This allows an easier assessment of differences between sites. In addition, the non-matrix Multi-Dimensional Scaling (MDS) maps (2013) were used to visualise the (dis)similarities between the large zircon datasets of Red Clay, loess and the potential source areas. This MDS technique was developed based on the Kolmogorov-Smirnov (KS) statistic to measure the dissimilarities between detrital zircon age distributions and provides an efficient and quantified way to compare large datasets (Vermeesch, 2013). Despite some limitations, such as inability of the KS effect to capture the full richness of the entire probability distributions and sensitivity to the strongest signal, this method is able to capture the main feature of the detrital zircon datasets and were well practiced in the provenance study of Red Clay and Quaternary loess (Bird et al., 2015; Che and Li, 2013; Nie et al., 2014; Stevens et al., 2013; Vermeesch, 2013). The quality of the KS statistic model (goodness-of-fit) is expressed by the "stress value", which are usually acceptable if less than 10% (Vermeesch, 2013). We used the newly released R package "Provenance" to plot the 2D MDS maps (seen from http://www.ucl.ac.uk/~ucfbpve/provenance/).

S.4. Backtrace air trajectory modelling

Compared to that using NCEP reanalysis data (the default input for HYSPLIT), the HYSPLIT model using our global model results as the input well capture the major directions of the trajectories in the study sites (Fig. S3). In particular, the spatial differences among the four sites, i.e., increasing northerly trajectories from Dongwan to Chaona, to Lantian and to Baode, are well reproduced. We note several differences between the results using our global model results and that using NCEP reanalysis data as the input data. For instance, when using our global model results as the input data for HYSPLIT, there are less trajectories crossing the western deserts (D and E) than that using NCEP reanalysis data (Fig. S3e and j). In addition, the trajectories in Baode and Lantian tend to reach higher altitude backward than that using NCEP reanalysis (Fig. S3). These discrepancies, however, do not affect the large-scale spatial patterns captured by HYSPLIT using our global model results. Therefore, it is reasonable to use our global model results as the input data for HYSPLIT to study the Late Miocene trajectories. As to the Late Miocene global model simulation used in this study, it has been shown to simulate the Late Miocene climate reasonably well compared to proxy data and other model simulations (Micheels et al., 2011). In terms of East Asian winter monsoon and

westerly wind, the global model we use (i.e. ECHAM5/MPIOM) seems to behave differently from other global models in simulating the mid-Pliocene climate. It tends to simulate stronger winter monsoon wind and less northward shift of westerly in the mid-Pliocene than other models (Zhang et al., 2013a; Li et al., 2015b). The modelling studies on the Late Miocene westerly and winter monsoon are very limited, but given the similar boundary conditions to the Pliocene, we could assume similar behaviour for our Late Miocene model experiments. As a result, our model may give rise to more trajectories from the north to the Loess Plateau than the other models in the Late Miocene for all four localities (see Fig. 7e). Nevertheless, we do not think such model behaviour may seriously bias the spatial pattern we observed in our model results, i.e., more northerly trajectories to the northern Loess Plateau than to the southern Loess Plateau.

S.5. Bulk grain size distributions of zircon samples

The grain-size distribution frequency plots (Fig. S1) from the Baode Fm are very distinctive and correspond well with the EM modelling results. For instance, the samples BD-1 (7.16 Ma) and BD-2 (6.91 Ma) from the lower part of the Baode Fm are characterised by high/large modal sizes at 44 and 70 μm, respectively, and show similar GSDs patterns to the fluvial sediments in the northern CLP (cf. Lu et al., 2001; Sun et al., 2002). Bulk grain-size distribution of the zircon samples from the upper part of the Baode Fm have polymodal GSDs spectra, interpreted as representing reworked aeolian Red Clay, and partly mixed with hydraulic sediment (cf. Sun et al., 2002). The GSDs of the bulk samples from the other sequences (Jingle Fm, Dongwan and main part of the Lantian Fm) are identical with the typical Red Clay deposits (cf. Lu et al., 2001; Sun et al., 2002; Sun et al., 2006b; Vandenberghe, 2013; Vandenberghe et al., 2004) by showing bimodal distributions and high percentages of fine component with the general fine modal sizes around ca. 11 μm. It is also noticed that the GSD of the sample LT-5 (5.83 Ma) from the lower part of the Lantian Fm shows a peak at a very coarse modal size (420 μm), which matches well with that of EM1 of the Lantian Fm, indicating a coarse fluvial component in this sample.

S.6. Zircon grain morphology

Although the majority of the zircons are 20 to 60 μm in length and mostly sub-angular to subrounded in shape, there are discernible distinctions in zircon sizes and shapes among different sections (Fig. S2). In general, zircon grains from Baode Red Clay are relatively coarser (30–60 μm) than those in the southern sections (i.e. Lantian and Dongwan) where the average zircon grain size is 20–40 μm. The number of euhedral crystals is also larger in the Baode sequence, especially in the Jingle Fm where the proportion of euhedral shapes exceeds 50%. The lowermost Lantian Fm sample LT-5 (5.83 Ma; Fig. S2e) is exceptional as it contains abundant zircon grains more than 60 μm in length and a very narrowly spaced age distribution. Among all the sites, over 30% of the zircons in the Red Clay are fractured or small fragments, in Dongwan (DW-1 and 4) even >50%.

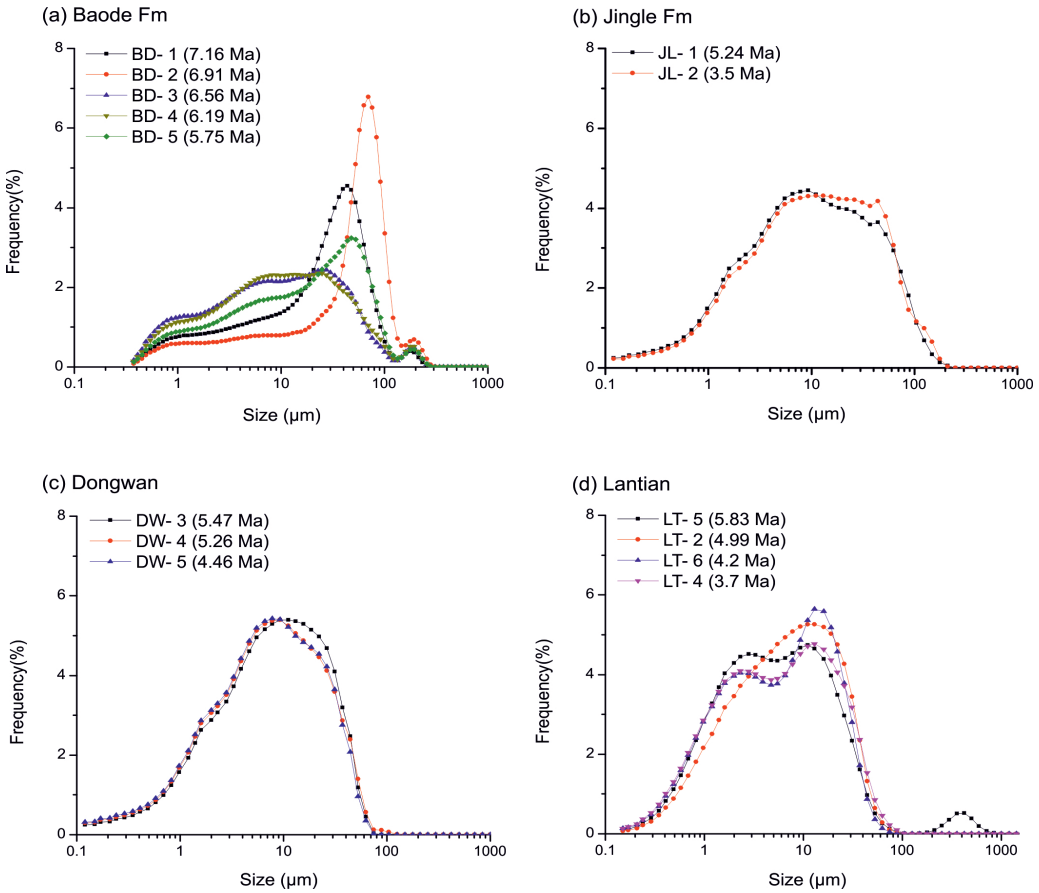

Figure S1. Bulk grain-size distribution of zircon samples from **(a)** Baode Fm, **(b)** Jingle Fm, **(c)** Dongwan and **(d)** Lantian Fm

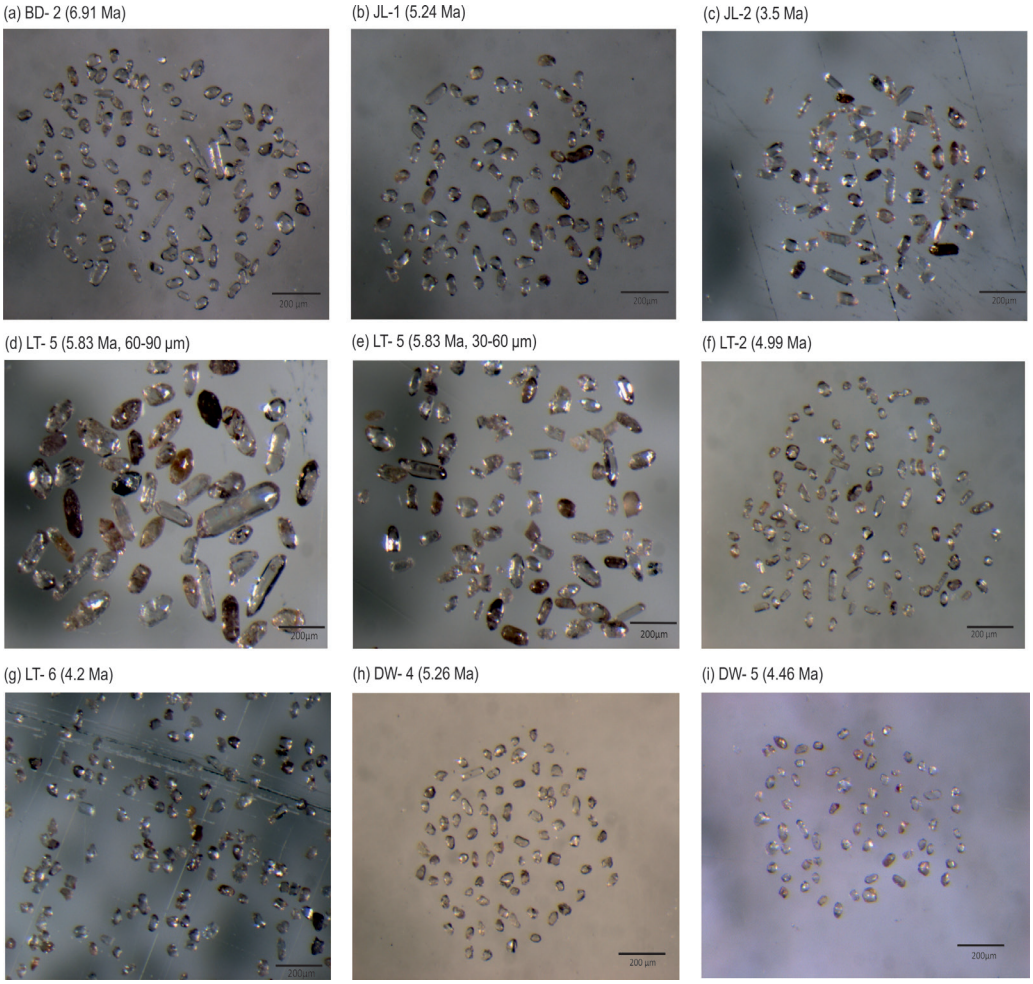

Figure S2. Photomicrographs of randomly selected zircon grains from Bao Fm **(a)**, Jingle Fm (**b** and **c**), Lantian (**d-g**) and Dongwan (**h** and **i**) samples.

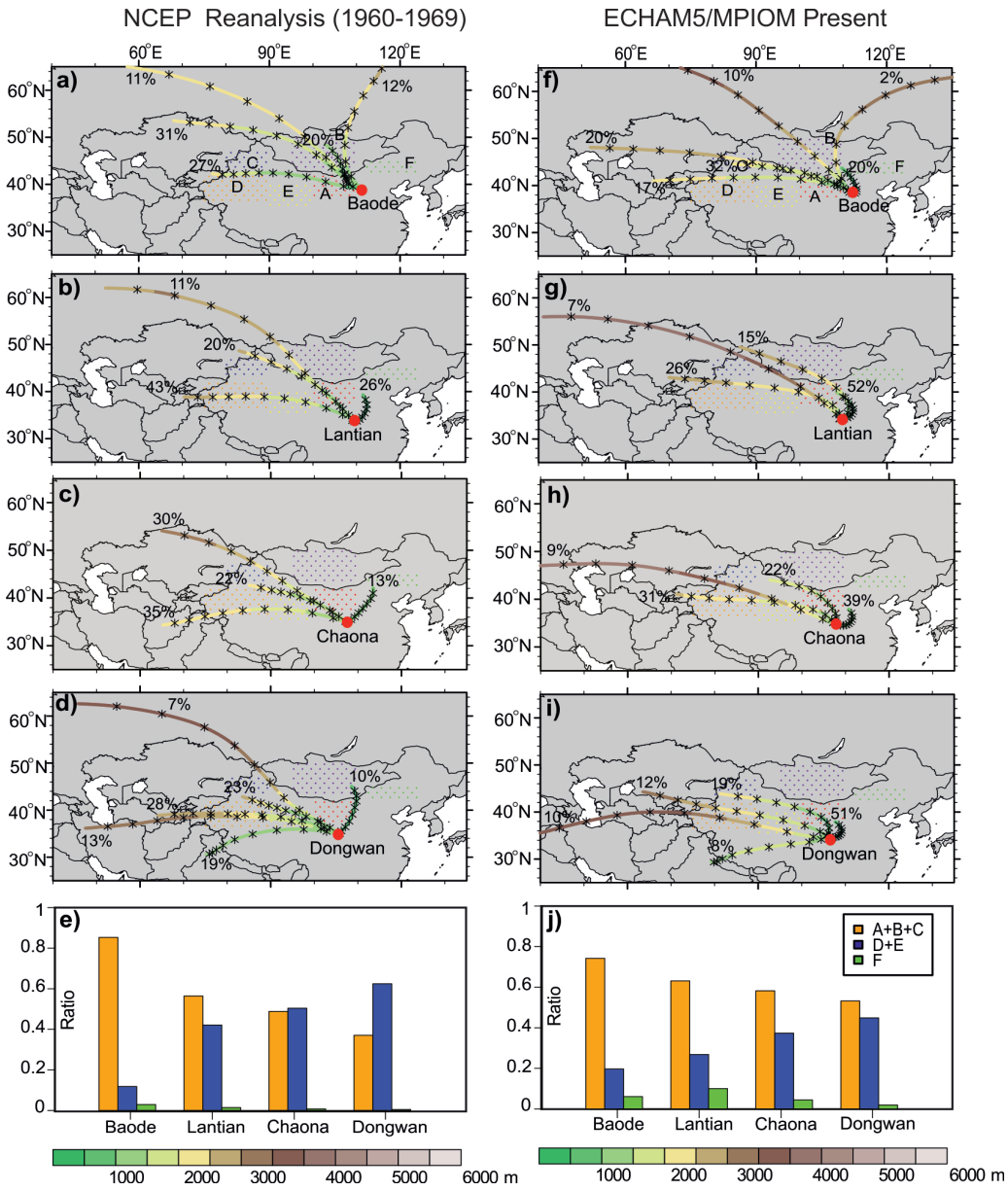

Figure S3. The cluster-mean 5-days backtrace trajectories in winter for the studied localities calculated by the HYSPLIT model using NCEP reanalysis data (Kalnay et al., 1996) **(a, b,c, d, e)** and present-day simulation from the global model experiments (Micheels et al., 2011) **(f, g, h, i, j)**, **(a, f)** Baode, **(b, g)** Lantian, **(c, h)** Chaona and **(d, i)** Dongwan. The colors of the trajectory denote its height and the asterisks denote the locations of air parcel at 12 hourly intervals. The number along each cluster-mean trajectory denotes the percentage of trajectories belong to the cluster. The coloured dotted areas denote the potential dust sources similar to that in Fig. 1: Northern Desert (red, A), Southern Mongolia Gobi Desert (purple, B), Junggar Basin (blue, C), Tarim Basin (orange, D), Northern Tibetan Plateau (yellow, E), Northeastern sandy lands (green, F). The ratios of the number of trajectories passing the northern desert (A, B, C), the western desert (D, E) and the eastern desert (F) for different localities are shown in (e, j).